Title

A pQCD - Based Approach to Parton Production and Equilibration in High-Energy Nuclear Collisions

Author

Wang, X.-N.

Publication Date

1996-01-20

LBL-38145
UC-413
Preprint

ERNEST ORLANDO LAWRENCE
BERKELEY NATIONAL LABORATORY

A pQCD-Based Approach to Parton Production and Equilibration in High-Energy Nuclear Collisions

X.-N. Wang
Nuclear Science Division

January 1996
Submitted to
Physics Reports

DISCLAIMER

LBL-38145

A pQCD-based Approach to Parton Production and Equilibration in High-Energy Nuclear Collisions*

XIN-NIAN WANG
Nuclear Science Division, Mailstop 70A-3307
Lawrence Berkeley National Laboratory
University of California, Berkeley, CA 94720 USA

Contents

*This work was supported by the Director, Office of Energy Research, Division of Nuclear Physics of the Office of High Energy and Nuclear Physics of the U.S. Department of Energy under Contract No. DE-AC03-76SF00098 and U.S. - Hungary Science and Technology Joint Fund J. F. No. 378

ABSTRACT

A pQCD-based model for parton production and equilibration in ultrarelativistic heavy-ion collisions is reviewed. The model combines pQCD processes including initial and final state radiations together with string phenomenology for nonperturbative soft processes. Nuclear effects on the initial parton production, such as multiple parton scattering and nuclear shadowing of parton distribution functions are considered. Comparisons with existing data are made and further tests of the model to constrain model parameters are proposed. With the obtained space-time history of the parton production, evolution of the minijet gas toward a fully equilibrated parton plasma is studied. Direct probes of the early parton dynamics, such as pre-equilibrium photon and dilepton production, open charm production, J/ψ suppression and jet quenching are also reviewed.

1 Introduction

According to the Big Bang theory, during the early stage of the evolution of our universe, there existed a state of matter consisting mainly of unbound quarks and gluons at a temperature of about 200 MeV. As the universe expanded and cooled down, it went through a phase transition and eventually evolved to what we see today. Such a phase transition was predicted [1, 2] shortly after Quantum Chromodynamics (QCD) was established as the fundamental theory for strong interactions. In this theory, quarks, which have three types of color charges, interact via non-Abelian gauge bosons, i.e., gluons. Because of the non-Abelian nature of strong interactions, quarks and gluons are confined to hadrons under normal circumstances. However, hadronic matter under extremely dense and hot conditions will go through a phase transition to form a quark-gluon plasma in which quarks and gluons are no longer confined to the size of a hadron. Lattice gauge studies of QCD at finite temperatures have indeed found such a phase transition, though the nature of the transition has not yet been clarified [3].

To recreate the early universe and experimentally verify the QCD phase transition in the laboratory, it was proposed that nuclei be accelerated to extremely high energies and then allowed to collide with each other. During the collisions, both high baryon densities and high temperatures might be reached. Thus, a quark-gluon plasma could be formed which will subsequently go through the phase transition and hadronize into particles in the final states. During the last decade, heavy-ion experiments have been done at the AGS of BNL and the SPS of CERN with $E_{\rm lab} \approx 14$ and 200 AGeV, respectively. The results from those experiments [4] have demonstrated extremely rich physics which cannot be explained by simple extrapolation of pp collisions. However, up to now, there is no unambiguous evidence for the existence of a quark-gluon plasma over a significantly large space-time region. While experiments at AGS and SPS and their analyses continue, new experiments [5] have been planned at RHIC of BNL and LHC of CERN with $E_{\rm cm} = 200$ AGeV and 5.5 ATeV, respectively. What I would like to emphasize in this review is that heavy-ion collisions at these ultrarelativistic energies will demonstrate a completely new dynamics which is not accessible at the present energies.

The key issue here is the nuclear structure at different scales. When the transverse momentum transfer involved in each nucleon-nucleon collision is small ($p_T \lesssim \Lambda_{\rm QCD}$), effective models based on, *e.g.*, meson-exchange and resonance formation are sufficient to describe multiple interactions between hadrons in which the parton structure of the hadrons cannot yet be resolved. These coherent (with respect to the partons inside the hadron) interactions lead to collective behavior in low-energy

heavy-ion collisions as were first observed in the Bevalac experiments [6] and recently at the AGS energies [7]. However, when p_T becomes large enough to resolve individual partons inside a nucleon, the dynamics is best described on the parton level via perturbative QCD (pQCD). Though hard parton interactions occur at CERN-SPS energies ($\sqrt{s} \lesssim$ 20 AGeV), they play a negligible role in the global features of heavy-ion collisions. However, at collider energies ($\sqrt{s} \gtrsim 100$ AGeV) the importance of hard or semihard parton scatterings is clearly seen in high-energy pp and $p\bar{p}$ collisions [8]. They are therefore also expected to be dominant in heavy-ion collisions at RHIC and LHC energies [9, 10]. These hard or semihard interactions happen on a very short time scale and they generally break color coherence inside the individual nucleons. After the fast partons pass through each other and leave the central region, a dense partonic system will be left behind which is not immediately in thermal and chemical equilibrium. The partons inside such a system will then further interact with each other and equilibration will eventually be established if the interactions are frequent enough among a sufficiently large number of initially produced partons. Due to the asymptotic behavior of QCD, production rates of hard and semihard partons are calculable via perturbative QCD during the initial stage of heavy-ion collisions. The color screening mechanism in the initially produced dense partonic system makes it also possible to use pQCD to investigate thermal and chemical equilibration of the system.

Currently, there are many models to describe the coherent hadronic interaction in which parton degrees of freedom are not important yet. In these models, hadrons remain as individual entities and particle production is mainly through resonance formation. Indeed, most of the experimental data at AGS energies can be explained by RQMD [11] and ARC [12] Monte Carlo simulations. As the colliding energy increases, partons inside nucleons become more relevant as the basic constituents of the interaction. However, nonperturbative soft interactions still dominate the collision dynamics in the energy range $\sqrt{s} \lesssim 100$ AGeV. In order to describe particle production in this energy range, phenomenological string models[13, 14, 15, 16] have been developed and they can explain well the global properties of particle production at CERN SPS energies. The physics behind these string models is that multiple partons produced in soft interactions are not independent of each other. Coherence among them can be modeled by strings or flux tubes between leading quarks and diquarks (or antiquarks). Particle production comes from the fragmentation of the string through $q\bar{q}$ creation inside the flux tube. At collider energies, $\sqrt{s} > 100$ AGeV, hard and semihard scatterings, which can be calculated via pQCD, become increasingly important. Since nonperturbative physics is always present in any processes involving strong interactions, pQCD has to be combined with models of nonperturbative inter-

actions, *e.g.*, string models. Such pQCD-inspired models, like PYTHIA [17], ISAJET [18], describe well the high p_T phenomena in high-energy hadronic collisions. Along the same line, M. Gyulassy and I extended this approach to high-energy heavy-ion collisions and developed the HIJING (Heavy Ion Jet INtercation Generator) Monte Carlo model [19] to take into account the physics of hard and semihard parton production. Nearly at the same time, similar models, PCM [20] and DTUNUC [21], also emerged. In particular, PCM has explicitly modeled the space-time evolution of the parton production processes and rescatterings along the lines of Boal [22]. Though hard and semihard processes become dominant at high energies, they are always accompanied by soft interactions. These soft interactions in general produce many soft final partons and take longer time (~ 1 fm/c) to complete. Therefore, they cannot be modeled by simple elastic parton-parton scatterings. However, these nonperturbative interactions might be modified inside a dense partonic medium, so that a perturbative method might be sufficient to describe the evolution of the initially produced dense partonic system towards an equilibrated quark-gluon plasma.

The crux of parton dynamics in heavy-ion collisions rests in the complexity of multiple parton scatterings and the associated bremsstrahlung. An exact quantum field treatment of these multiple parton interactions must include all possible matrix elements and the interference between them. Although quantum transport theory [23, 24, 25] can in principle include all these interference effects and developments in this subject are impressive in the last few years, its applicability to heavy-ion collisions is still far from being realistic. An alternative and more realistic solution to this problem is to find ways to incorporate correctly the subtle interference phenomena in a *classical* parton cascade model. There are two important interference phenomena in multiple parton interactions. (1) The interference among different amplitudes of multiple parton scatterings, especially in the initial parton scatterings when the two beams of fast partons pass through each other, leads to the Glauber formula of multiple interactions [26, 27]. Thus, a semiclassical cascade cannot be used to treat the initial parton production during the overlapping period of the two colliding nuclei. The resultant interference is responsible, as I will demonstrate later, for the disappearance of the nuclear enhancement of jet production in pA collisions at large p_T and high energies. Therefore, we can neglect processes in which a parton suffers multiple hard scatterings in the initial parton scatterings. Brodsky and Lu have shown [28] that a Glauber analysis of multiple antiquark-nucleon scatterings also leads to nonperturbative shadowing of the quark distributions inside heavy nuclei. (2) The spectrum of induced gluon bremsstrahlung in multiple scatterings is also modified by the destructive interference among different radiation amplitudes, the so-called Landau-Pomeranchuk-Migdal (LPM) effect [29, 30]. In a detailed analysis [27, 31],

one finds that the interference actually happens between two amplitudes in which the beam parton has completely different virtualities, *i.e.*, time-like in the final state radiation of one scattering and space-like in the initial state radiation of the previous one. Therefore, a propagating parton can no longer be considered as *always* time-like with a decreasing virtuality in a parton cascade simulation, *e.g.*, PCM [20].

Another aspect of parton production and interaction in ultrarelativistic heavy-ion collisions is that the same processes responsible for parton equilibration can also provide direct probes of the early parton dynamics and the properties of the parton gas during its evolution toward a fully equilibrated quark-gluon plasma. For example, parton scatterings in an equilibrating system also lead to dilepton, photon and charmed quark production. Since the production rates of these three processes are proportional to the product of quark-quark, quark-gluon and gluon-gluon densities, respectively, measurements of the thermal enhancement of dileptons, photons and charmed quarks can provide us with information of the quark and gluon densities in the plasma, and thus on the thermal and chemical equilibration. Interactions of an initially produced high-p_T jet with partons inside the equilibrating plasma, in the meantime, will cause the jet losing energy. Studying of jet quenching due to energy loss can thus tell us whether and how the the parton gas is thermalized. Because of the same mechanism, J/ψ is also suppressed due to its interaction with the parton gas. Since the J/ψ dissociation cross section inside a deconfined partons is very different from that inside a hadronic gas, the study of J/ψ suppression can then provide us with evidence for color deconfinement in the parton plasma and possibly with information on the QCD phase transition.

This review will be structured as follows: In the next section, I will review a pQCD-inspired model for multiple parton production in pp, pA and AA collisions. Special emphasis will be devoted to the role of hard and semihard parton collisions and their connection to Pomeron structure and soft interactions. I will also discuss the interpolation between hard and soft physics and the possible treatment of non-perturbative interactions. In Section 3, nuclear effects such as multiple initial and final state interactions and nuclear shadowing of parton distribution functions will be discussed. The Monte Carlo implementation of parton production will also be reviewed. In Section 4, I will discuss the evolution of a partonic system via pQCD, including the Landau-Pomeranchuk-Migdal (LPM) effect on induced gluon radiation. In Section 5, I will discuss the possibility of using hard processes as probes of the early parton dynamics, the formation of quark-gluon plasma formation and the QCD phase transition. In particular, photon and dilepton production, charm production, pre-equilibrium J/ψ suppression, jet quenching, and monojet production will be discussed. Finally I will give a summary and discussion in Section 6.

2 Parton Scatterings in Hadron-Hadron Collisions

High-energy nuclear collisions are expected to be dominated by semihard parton collisions with transverse momentum transfers $p_T \gtrsim p_0 \sim 1 - 2$ GeV/c. The produced partons carrying such transverse momenta are often referred to as minijets. Multiple parton production has been estimated[10] to produce up to 50% (80%) of the transverse energy per unit rapidity in the collisions of heavy nuclei at RHIC (LHC) energies. While not resolvable as distinct jets, minijets are expected to lead to a wide variety of correlations among observables, such as transverse momentum, strangeness and fluctuation enhancements, that compete with expected signatures of a QGP. Therefore, it is especially important to calculate these background processes as reliably as possible. In addition, it has been shown that multiple mini-jet production is important in $p\bar{p}$ interactions to account for the increase of the total cross section[33] with energy, the increase of the average transverse momentum with charged multiplicity[34], and the violation of Koba-Nielsen-Olesen (KNO) scaling of the charged multiplicity distributions[17, 35].

It has long been recognized [33] that the inclusive jet cross section $\sigma_{\rm jet}$ in pp or $p\bar{p}$ collisions increases very rapidly with energy and eventually will be larger than the total inelastic cross section $\sigma_{\rm in}$. This is because the inclusive jet cross section also contains the average number of jets per inelastic event. Thus,

$$\sigma_{\rm jet} = \langle n_{\rm jet} \rangle \sigma_{\rm in}, \tag{1}$$

where $\langle n_{\rm jet} \rangle$ is the average number of hard or semihard scatterings per inelastic event. One way to include hard or semihard processes in the unitarized cross sections of pp and $p\bar{p}$ is to introduce the idea of Pomeron exchanges in an eikonal formalism. I will argue that hard or semihard scatterings can be considered as the hard loops inside a Pomeron exchange, and the interpolation between hard and soft components will become clear. This will also shed some light on the modeling of the soft component.

2.1 Pomeron Exchange and Minijet Production

The Pomeron was introduced to describe the effective interaction between quarks and gluons [36, 37, 38]. It has been used to model hadronic cross sections, diffractive interactions and multiple particle production. In general, it is considered to be a color singlet object with the quantum numbers of a photon. It can couple both to quarks and gluons. The imaginary part of a Pomeron exchange amplitude is usually related to multiple particle production in hadronic interactions. Let us first consider the eikonal formalism for quark scatterings via multiple Pomeron exchange.

Denote the matrix element for a single Pomeron exchange as

$$\mathcal{M}_{\rm el}^{(1)} = 2\pi i\delta(E_i - E_f)2\pi\sqrt{s}f_1(s,t), \tag{2}$$

$$\begin{aligned} f_1(s,t) &= \frac{-i}{2\pi}\frac{g_p}{i\sqrt{s}}\bar{u}_{\sigma_f}(p_f)\,\not{A}(\mathbf{q})u_{\sigma_i}(p_i) \\ &\equiv \frac{-i}{2\pi}\frac{1}{i\sqrt{s}}T(s,\mathbf{q}), \end{aligned} \tag{3}$$

where $\sqrt{s}/2 = E_i = E_f$ and g_p is a coupling constant between a quark and a Pomeron. The amplitude $f(s,t)$ is defined such that the differential cross section for elastic scatterings is given by

$$\frac{d\sigma}{dt} = \pi|f(s,t)|^2. \tag{4}$$

The initial and final polarizations, σ_i, σ_f, should be averaged and summed over in the calculation of the cross sections. One can check that if $A(\mathbf{q})$ is replaced by a Debye screened Coulomb potential, $A(\mathbf{q}) = g/(\mathbf{q}^2+\mu^2)$, and g by the strong coupling constant, the above formula leads to $d\sigma/dt = 4\pi\alpha_s^2/(\mathbf{q}^2+\mu^2)^2$.

One can similarly write down the amplitude for double Pomeron exchange,

$$\begin{aligned} \mathcal{M}_{\rm el}^{(2)} = 2\pi i\delta(E_i - E_f)(-g_p^2) \int \tfrac{d^3\ell}{(2\pi)^3}\bar{u}_{\sigma_f}(p_f)\,\not{A}(\mathbf{p}_f - \ell)\tfrac{\not{\ell}}{\ell^2+i\epsilon}\,\not{A}(\ell - \mathbf{p}_i)u_{\sigma_i}(p_i) \\ e^{-i(\ell-\mathbf{p}_i)\cdot\mathbf{x}_1 - i(\mathbf{p}_f-\ell)\cdot\mathbf{x}_2}, \end{aligned} \tag{5}$$

where energy conservation at each coupling vertex sets the energy of the internal line to $\ell^0 = \sqrt{s}/2 = E_f$. Amplitudes involving backscattering are suppressed at high energies, because of the limited momentum transfer that each the Pomeron can impart. If we assume that Pomerons do not overlap in space, the singularity in $A(\mathbf{q})$ can be neglected, and the integration over ℓ_z (with respect to the $\hat{z}$ direction of $\mathbf{x}_{21} = \mathbf{x}_2 - \mathbf{x}_1 = L\hat{z} + \mathbf{r}_\perp$) gives us

$$\begin{aligned} \mathcal{M}_{\rm el}^{(2)} &= 2\pi i\delta(E_i - E_f)\int\frac{d^2\ell_\perp}{(2\pi)^2}\bar{u}_{\sigma_f}(p_f)(-g_p^2)\Gamma_{(2)}u_{\sigma_i}(p_i), \\ \Gamma_{(2)} &= \not{A}(\mathbf{p}_f - \mathbf{p})\frac{\not{p}}{2ip_z}\not{A}(\mathbf{p} - \mathbf{p}_i)e^{-i(\mathbf{p}-\mathbf{p}_i)\cdot\mathbf{x}_1 - i(\mathbf{p}_f-\mathbf{p})\cdot\mathbf{x}_2}, \end{aligned} \tag{6}$$

where $p = (E_f, \sqrt{E_f^2 - \ell_\perp^2}, \ell_\perp)$ is the four-momentum of the internal line. One can derive the classical Glauber multiple collision cross section from this amplitude by averaging and summing over the initial and final state ensemble of the target[27]. In the limit of high-energy and small angle scattering, one can neglect the phase factor

in the above equation and obtain the amplitude [as defined in Eq. (2)],

$$f_2(s,t) = \frac{-i}{2\pi}\int d^2b \frac{1}{2!}[-\chi(\mathbf{b},s)]^2 e^{i\mathbf{q}_\perp\cdot\mathbf{b}}, \tag{7}$$

where $1/2!$ comes from the different orderings of the target potentials and $\mathbf{q}_\perp = \mathbf{p}_{f\perp} - \mathbf{p}_{i\perp}$ is the total transverse momentum transfer from the multiple scatterings. The eikonal function $\chi_{\sigma_1,\sigma_2}(\mathbf{b},s)$ is defined as the Fourier transform of the single scattering amplitude (besides a factor $i/2\pi$),

$$\begin{aligned}\chi(\mathbf{b},s) &\equiv \frac{i}{\sqrt{s}}\int \frac{d^2q_\perp}{(2\pi)^2} e^{-i\mathbf{q}_\perp\cdot\mathbf{b}} T(s,\mathbf{q}_\perp) \\ &= \frac{i}{4\pi\sqrt{s}}\int_{-\infty}^{0} dt J_0(b\sqrt{-t}) T(s,t),\end{aligned} \tag{8}$$

where $t = -\mathbf{q}_\perp^2$ and J_0 is the zeroth order Bessel function. In the definition of the product of eikonal functions, summation over the polarizations of the intermediate lines is implied. If we are only interested in unpolarized collisions, we can regard $T(s,\mathbf{q}_\perp)$ as a scalar in the following. One can generalize the double scattering amplitude to multiple scatterings and sum them together to get the total amplitude,

$$\begin{aligned}f(s,t) = \sum_{n=1}^{\infty} f_n(s,t) &= \frac{-i}{2\pi}\int d^2b \sum_n \frac{1}{n!}[-\chi(\mathbf{b},s)]^n e^{i\mathbf{q}_\perp\cdot\mathbf{b}} \\ &= \frac{i}{2\pi}\int d^2b [1 - e^{-\chi(\mathbf{b},s)}] e^{i\mathbf{q}_\perp\cdot\mathbf{b}}.\end{aligned} \tag{9}$$

This is the total elastic quark scattering amplitude in the eikonal formalism. This amplitude can also be derived from the scattering theory in quantum mechanics [39], where the eikonal function is related to the potential experienced by the scattering particle.

One can consider a *pp* interaction as multiple quark-quark scatterings and derive a similar formula for the total amplitude of an elastic *pp* collision. The effective eikonal function for *pp* collisions now should be given by

$$\chi(\mathbf{b},s) = \frac{i}{\sqrt{s}}\int \frac{d^2q_\perp}{(2\pi)^2} e^{-i\mathbf{q}_\perp\cdot\mathbf{b}} t(\mathbf{q}_\perp,s) t(-\mathbf{q}_\perp,s) T(s,\mathbf{q}_\perp), \tag{10}$$

where $t(\mathbf{q}_\perp,s)$ is the Fourier transform of the quark density distribution inside a nucleon and $T(s,\mathbf{q}_\perp)$ is the amplitude of a quark-quark scattering with one Pomeron exchange. Here we neglected the contribution from Reggeon exchanges, so that the amplitude $T(s,\mathbf{q}_\perp)$ is purely imaginary [28] (or the eikonal function is real); thus

the elastic amplitude of pp collisions, Eq.(9), is also purely imaginary. Experimental measurements of high-energy pp or $p\bar{p}$ collisions indeed find the real part of the elastic amplitude to be small [40].

With the above elastic amplitude, the differential elastic cross section for pp collisions is given by Eq. (4). Using the identity

$$\int_{-\infty}^{0} dt J_0(b\sqrt{-t}) J_0(b'\sqrt{-t}) = \frac{2}{b}\delta(b-b'), \tag{11}$$

one can obtain the elastic cross section,

$$\sigma_{\rm el} = \int d^2b \left[1 - e^{-\chi(b,s)}\right]^2, \tag{12}$$

where we assumed that the imaginary part of the eikonal function is negligible. Using the optical theorem, one can also get the total and inelastic cross sections of pp collisions[35, 41],

$$\sigma_{\rm tot} = 4\pi {\rm Im} f(s,t=0) = 2\int d^2b \left[1 - e^{-\chi(b,s)}\right], \tag{13}$$

$$\sigma_{\rm in} = \sigma_{\rm tot} - \sigma_{\rm el} = \int d^2b \left[1 - e^{-2\chi(b,s)}\right]. \tag{14}$$

The approximation of a small imaginary (real) part of the eikonal function (elastic amplitude) in Eq. (10) also leads us to assume that the quark-quark scattering amplitude $T(s,\mathbf{q}_\perp)$ with one Pomeron exchange is also purely imaginary [cf. Eqs. (9) and (10)]. According to Eq. (3) and the optical theorem , $T(s,\mathbf{q}_\perp)$ should be related to the total inclusive cross section of quark-quark scatterings,

$$T(s,\mathbf{0}) = -i\frac{\sqrt{s}}{2}\sigma_{\rm incl}(s). \tag{15}$$

Assuming the dominance of small angle contributions in Eq. (10), we have then the eikonal function for pp collisions,

$$\chi(b,s) \approx \frac{1}{2}\sigma_{\rm incl}(s) T_N(b,s), \tag{16}$$

where $T_N(b,s)$ is the overlap function of two nucleons,

$$T_N(b,s) = \int d^2b' t(\mathbf{b}',s) t(\mathbf{b}-\mathbf{b}',s), \tag{17}$$

which is normalized to one, $\int d^2b T_N(b,s) = 1$.

2.2 Cross Sections: Soft vs. Hard

To calculate the total inclusive cross section of quark-quark scatterings, $\sigma_{\rm incl}(s)$, one needs to know the Pomeron structure and its coupling to quarks and gluons. In a simple model, one can regard a Pomeron as a double gluon exchange with a ladder structure as illustrated in Fig. 1(a). In general, most of the loops inside the ladder have soft momenta and thus cannot be calculated via pQCD. We consider this non-perturbative contribution to the inclusive cross section as $\sigma_{\rm soft}(s)$. As the colliding energy $\sqrt{s}$ increases, contributions from large momentum, $p_T > p_0$, to the loop integral also increase. As illustrated in Fig. 1(b), the cutting diagram of such a Pomeron exchange which contains at least one hard loop corresponds to hard scatterings in pp collisions. If one assumes that the loop momenta are ordered so that they increase toward the hard loop, then the rest of the cut-Pomeron beside the hard loop can be resummed to give the quark or gluon (parton) distributions of a nucleon and their Gribov-Lipatov-Altarelli-Parisi (GLAP) [42] evolution. The corresponding contribution to the inclusive cross section can then be identified as the inclusive jet cross section [43],

$$\sigma_{\rm jet} = \int_{p_0^2}^{s/4} dp_T^2 dy_1 dy_2 \frac{1}{2} \frac{d\sigma_{\rm jet}}{dp_T^2 dy_1 dy_2}, \tag{18}$$

$$\frac{d\sigma_{\rm jet}}{dp_T^2 dy_1 dy_2} = K \sum_{a,b} x_1 f_a(x_1, p_T^2) x_2 f_b(x_2, p_T^2) \frac{d\sigma^{ab}(\hat{s}, \hat{t}, \hat{u})}{d\hat{t}}, \tag{19}$$

where the summation runs over all parton species, y_1 and y_2 are the rapidities of the scattered partons, and x_1 and x_2 are the light-cone momentum fractions carried by the initial partons. These variables are related by $x_1 = x_T(e^{y_1} + e^{y_2})/2$, $x_2 = x_T(e^{-y_1} + e^{-y_2})/2$, $x_T = 2p_T/\sqrt{s}$. The $f_a(x, Q^2)$ in Eq. (19) are the parton distribution functions. The pQCD cross sections, $d\sigma_{ab}$, depend on the subprocess variables $\hat{s} = x_1 x_2 s$, $\hat{t} = -p_T^2(1 + \exp(y_2 - y_1))$, and $\hat{u} = -p_T^2(1 + \exp(y_1 - y_2))$. A factor $K \approx 2$ is included to correct the lowest order pQCD rates for next to leading order effects [44, 45].

At small $x \sim p_T/\sqrt{s}$, the momentum in the ladder diagram might not be ordered anymore and there might be more than one hard loop inside the ladder. However, calculations [46] have shown that such contributions are still small at present and future collider energies. If we neglect contributions from multiple hard loops , the total inclusive quark-quark cross section can be written as

$$\sigma_{\rm incl} = \sigma_{\rm soft}(s) + \sigma_{\rm jet}(s). \tag{20}$$

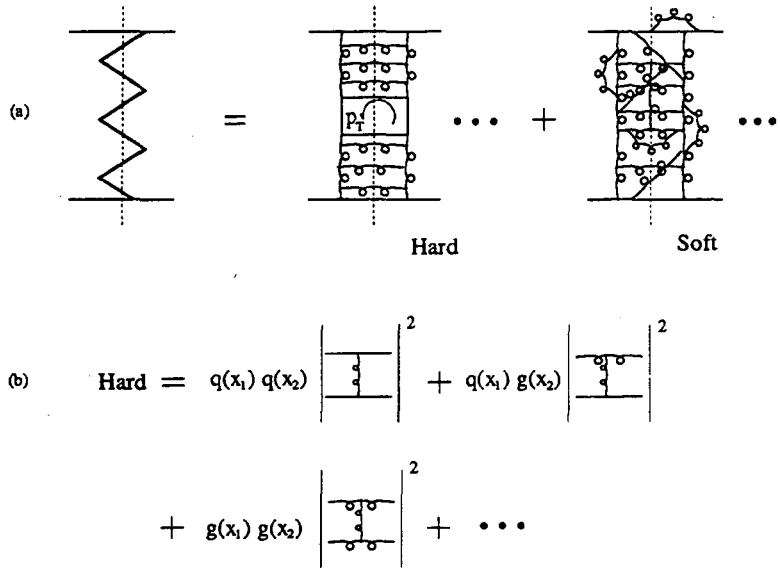

Figure 1: (a) A Pomeron can be divided into the ladder diagrams of a hard part, in which at least one loop momentum p_T is large, and a corresponding soft part. (b) The hard part of a cut-Pomeron can be factorized into parton distributions and hard scattering matrix elements.

where $\sigma_{\rm soft}$ represents the contribution from the cut-Pomeron in which the transverse momenta of the loops are limited to $p_T < p_0$, and therefore is not calculable via pQCD. However, as we can see from its definition, $\sigma_{\rm soft}$ represents processes involving many soft partons in the final state. It cannot be modeled by a simple two parton elastic scattering. Since there is no ordering in p_T, interference becomes important in soft particle production, which can be modeled by, *e.g.*, a string model.

Given the above decomposition of the total inclusive cross section and the eikonal function in Eq. (16), we can rewrite the inelastic cross section for pp collisions, Eq. (14), as

$$\sigma_{\rm in} = \int d^2b[1 - e^{-(\sigma_{\rm soft}+\sigma_{\rm jet})T_N(b,s)}] \equiv \int d^2b \sum_{j=0}^{\infty} g_j(b); \tag{21}$$

$$g_j(b) = \frac{[\sigma_{\rm jet}T_N(b,s)]^j}{j!} e^{-\sigma_{\rm jet}T_N(b,s)}, \quad j \geq 1; \tag{22}$$

$$g_0(b) = [1 - e^{-\sigma_{\rm soft}T_N(b,s)}]e^{-\sigma_{\rm jet}T_N(b,s)}. \tag{23}$$

where $g_j(b)$ can be considered as the probability for j hard scatterings [35, 47] among inelastic collisions at fixed impact paramenter b. Note that a jet in our terminology refers to a large p_T hard scattering. The average number of jets with $p_T \geq p_0$

in pp collisions is thus $\langle n_{\rm jet}\rangle = \sigma_{\rm jet}/\sigma_{\rm in}$. The above probabilistic interpretation of multiple hard scatterings depends on our assumption that multiple cut-Pomerons are independent from each other. This holds as long as the average number of hard scatterings is not too large. Given an interaction transverse area, $\sim \pi/p_0^2$, for processes with $p_T \sim p_0$, independence requires that the total interaction area is less than πR_N^2, where $R_N \approx 0.85$ fm is the nucleon radius; *i.e.*,

$$\sigma_{\rm jet} \lesssim (p_0 R_N)^2 \sigma_{\rm in} \equiv \sigma_{\rm max} \ . \tag{24}$$

For $p_0 \gtrsim 2$ GeV/c, and $\sigma_{\rm in} \approx 40$ mb, the right hand side is $\sigma_{\rm max} \approx 3$ barns, and thus the independent approximation should hold up to the highest energies foreseen. For nuclear collisions the total number of jets is given by

$$N_{\rm jet}^{AA} = T_{AA}(b)\sigma_{\rm jet} \ , \tag{25}$$

where $T_{AA}(b)$ is the nuclear overlap function at an impact parameter b. For $b = 0$, $T_{AA} \approx A^2/\pi R_A^2$, and multiple mini-jets may be independent as long as

$$\sigma_{\rm jet} \lesssim (p_0 R_A)^2 \pi R_A^2/A^2 \approx 2\sigma_{\rm max}/A^{2/3} \ . \tag{26}$$

For $A = 197$ the right hand side is 180 mb, and thus independence should apply up to LHC energies (see Fig. 2 below). On the other hand, nuclear shadowing of the initial structure functions will reduce the jet cross section so that independence should be valid beyond LHC energies.

For $p_0 > 1$ GeV, $\sigma_{\rm jet}(s)$ is found to be very small when $\sqrt{s} \lesssim 20$ GeV and only the soft component is important. The low-energy data of diffractive nucleon-nucleon scatterings exhibit a number of geometrical scaling properties[48] in the range $10 < \sqrt{s} < 100$ GeV, *e.g.*, $\sigma_{\rm el}/\sigma_{\rm tot} \cong 0.175$, and $B/\sigma_{\rm tot} \cong 0.3$, where B is the slope of the diffractive peak of the differential elastic cross section. This suggests a geometrical scaling form [49] for the eikonal function at low energies; *i.e.*, it is only a function of $\xi = b/b_0(s)$, with $\pi b_0^2(s) \equiv \sigma_{\rm soft}(s)/2$ providing a measure of the geometrical size of the nucleon. We further assume that the nucleon overlap function is given by the Fourier transform of a dipole form factor so that,

$$T_N(b,s) = \frac{\chi_0(\xi)}{\sigma_{\rm soft}(s)}; \tag{27}$$

$$\chi_0(\xi) = \frac{\mu_0^2}{48}(\mu_0\xi)^3 K_3(\mu_0\xi), \ \ \xi = b/b_0(s), \tag{28}$$

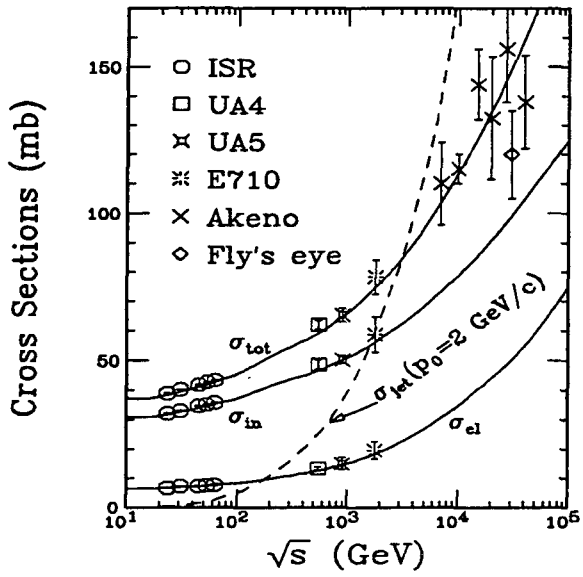

Figure 2: The total, inelastic, and elastic cross sections of pp and $p\bar{p}$ collisions calculated by HIJING (solid lines) as compared to the data [48, 50, 51, 52, 53, 54]. The dashed line is the total inclusive jet cross section with $p_T \geq p_0 = 2$ GeV/c.

where $\mu_0 = 3.9$. With this assumption, the eikonal function can be written as,

$$\chi(b,s) \equiv \chi(\xi,s) = \chi_0(\xi)[1 + \sigma_{\rm jet}(s)/\sigma_{\rm soft}(s)] \,. \tag{29}$$

This form ensures that geometrical scaling[49] is recovered at low energies when $\sigma_{\rm jet} \ll \sigma_{\rm soft}$.

Choosing $p_0 \simeq 2$ GeV/c and assuming a constant value of $\sigma_{\rm soft} = 57$ mb at high energies, the calculated cross sections and the multiplicity distributions in pp and $p\bar{p}$ collisions agree well with experiments[35]. This is the model adopted in HIJING [19] to simulate multiple jet production at the level of nucleon-nucleon collisions. In Fig. 2, the calculated total, inelastic and elastic cross sections of pp or $p\bar{p}$ collisions are shown as functions of $\sqrt{s}$ (solid line) together with experimental data[48, 50, 51, 52, 53, 54]. The dashed line corresponds to the inclusive jet cross section. The calculated cross sections agree well with experiments from ISR to Tevatron and cosmic-ray energies. We note that the total inclusive jet cross section increases much faster than the inelastic cross section as a function of $\sqrt{s}$, leading to an increase of the average number of minijets, $\sigma_{\rm jet}/\sigma_{\rm in}$, with energy.

We emphasize that the value of $p_0 = 2$ GeV used in the above calculation is only a phenomenological parameter. In order for the model to have some predictive power, p_0 should not depend on $\sqrt{s}$. However, its value is subject to considerable

controversy[33]. The problem arises from the fact that there is not a clear boundary specified by p_0 between soft and hard processes, as shown in Eqs. (18) and (20). If we believe that pQCD can be reliably applied to calculate hard contributions to the total inclusive cross section up to p_0, then the rest must be modeled by a phenomenological $\sigma_{\rm soft}$. Clearly, $\sigma_{\rm soft}(s)$ must depend on the choice of p_0. With a smaller (larger) p_0, more (less) contributions are included as hard collisions. Hence $\sigma_{\rm soft}(s)$ would be smaller (larger). Obviously many choices of p_0 and $\sigma_{\rm soft}(s)$ can give the same total cross section $\sigma_{\rm tot}(s)$. The only restriction is that the sum $\sigma_{\rm soft}(s) + \sigma_{\rm jet}(s)$ must have the right value to give the right energy dependence of the total cross section $\sigma_{\rm tot}(s)$. Since $\sigma_{\rm jet}(s)$ increases with decreasing p_0 and $\sigma_{\rm soft}(s)$ is non-negative, p_0 must be bounded from below by the experimental data on the total cross section $\sigma_{\rm tot}(s)$. We find that this lower limit in our model is $p_0 = 1.2$ GeV with the given parton distribution functions. For p_0 smaller than 1.2 GeV, the inclusive jet cross section at high energies is overestimated and the resultant $\sigma_{\rm tot}(s)$ can never fit the data. In addition, one must keep in mind that the lowest p_0 is also bounded by the relevant $Q_0 = p_0$ in the evolution of the parton distribution functions.

In HIJING, the parton distribution functions are taken to be the Duke-Owens[55] parametrization set 1 with $Q_0 = 2$ GeV. The latest version of this parameterization (DO1.1) for $f_a(x, Q^2)$ is adequate through RHIC energies. However, at higher energies, more updated distributions, such as GRV [56] or MRSD$-'$ [57] should be used. These distributions, constrained by the most recent HERA data [58] in deeply inelastic ep collisions, are more divergent at small x and give rise to larger minijet cross sections, especially at the LHC energy [59]. Using these distributions, one cannot fit $\sigma_{\rm tot}(s)$ at high energies with fixed p_0. As has been discussed in Ref. [46], this is due to multiple hard loops in one Pomeron exchange. The divergent behavior of the distribution functions is usually related to the fact that the hard loops are not ordered in p_T, which gives rise to multiple jet pair production per cut-Pomeron. Thus the inclusive jet cross section in the eikonal function must be normalized by the average number of such jet pairs [60].

2.3 Modeling the Soft Interactions

From Fig. 1(a), we can see that a cut-Pomeron always produces many soft partons with small transverse momenta no matter whether there is a hard process present or not. Unlike partons from initial and final state radiations associated with a hard scattering, these soft partons are not ordered in transverse momentum and coherence is extremely important, which could virtually produce a coherent color field. Therefore, soft interactions may not be modeled simply by regularized parton-parton elastic scatterings with small transverse momentum transfers. On the other hand,

the color field could also be screened significantly later by the interaction with the hard or semihard partons from the hard collisions [61] in heavy-ion collisions. The screening effect will decrease the final particle production from the color field.

As demonstrated in three-jet events in e^+e^- annihilations, the color interference effects can be approximated fairly well by a string model [62]. In HIJING we adopted a variant of the multiple string phenomenological model for the soft interaction as developed in Refs. [13, 14, 16]. Those soft interactions must naturally involve small p_T transfer to the constituent quarks, as well as induced soft gluon radiation which can be modeled by introducing kinks in the strings. The produced partons are treated either as hard kinks (for gluons) on the string or the end points (for quarks) of another string. The strings are assumed to decay independently via quark-antiquark creation using, in our case, the Lund JETSET7.2 [63] fragmentation routine to describe the hadronization.

The string excitation is achieved by a collective momentum transfer $P = (P^+, P^-, \mathbf{p}_T)$ between the hadrons. Given initial light-cone momenta

$$p_1 = (p_1^+, \frac{m_1^2}{p_1^+}, \mathbf{0}_T), \quad p_2 = (\frac{m_2^2}{p_2^-}, p_2^-, \mathbf{0}_T), \tag{30}$$

with $(p_1^+ + m_2^2/p_2^-)(p_2^- + m_1^2/p_1^+) \equiv s$, the final momenta of the strings are assumed to be

$$p_1' = (p_1^+ - P^+, \frac{m_1^2}{p_1^+} + P^-, \mathbf{p}_T), \quad p_2' = (\frac{m_2^2}{p_2^-} + P^+, p_2^- - P^-, -\mathbf{p}_T). \tag{31}$$

The remarkable feature of soft interactions is that low transverse momentum exchange processes with $p_T \lesssim 1$ GeV/c can result in large effective light-cone momentum exchanges[13], giving rise to two excited strings with large invariant mass. Defining

$$P^+ = x_+\sqrt{s} - \frac{m_2^2}{p_2^-}, \quad P^- = x_-\sqrt{s} - \frac{m_1^2}{p_1^+}, \tag{32}$$

the excited masses of the two strings will be

$$M_1^2 = x_-(1-x_+)s - p_T^2, \quad M_2^2 = x_+(1-x_-)s - p_T^2, \tag{33}$$

respectively. In HIJING, we require that the excited string mass must exceed a minimum value $M_{\rm cut} = 1.5$ GeV, and therefore the kinematically allowed region of $x^\pm$ is restricted to

$$x_-(1-x_+) \geq M_{Tcut1}^2/s, \quad x_+(1-x_-) \geq M_{Tcut2}^2/s, \tag{34}$$

where $M_{T\text{cut1}}^2 = M_{\text{cut}}^2 + p_T^2$, $M_{T\text{cut2}}^2 = M_{\text{cut}}^2 + p_T^2$. Only collisions with

$$s \geq s_{min} = (M_{T\text{cut1}} + M_{T\text{cut2}})^2 \tag{35}$$

are allowed to form excited strings. Eq. (35) also determines the maximum p_T that the strings can obtain from the soft interactions. In events with both hard and soft processes, two strings are still assumed to form but with a kinetic boundary reduced by the hard scatterings.

In HIJING, the probability for light-cone momentum transfer is assumed to be

$$P(x_\pm) = \frac{(1.0 - x_\pm)^{1.5}}{(x_\pm^2 + c^2/s)^{1/4}} \tag{36}$$

for nucleons and

$$P(x_\pm) = \frac{1}{(x_\pm^2 + c^2/s)^{1/4}[(1 - x_\pm)^2 + c^2/s]^{1/4}} \tag{37}$$

for mesons, with $c = 0.1$ GeV, along the lines of the DPM model[14]. Soft gluon bremsstrahlung processes with $p_T < p_0$ are also introduced as kinks along the excited string. In addition, HIJING also includes an extra low $p_T < p_0$ transfer to the constituent quarks and diquarks at the string end points in soft interactions. This effect is important at low energies, $E_{\text{lab}} \sim 20$ GeV, to account for the high p_T tails of the pion and proton distributions [19].

I emphasize that the low p_T algorithm used in HIJING is a phenomenological model needed to incorporate non-perturbative aspects of beam jet physics. Many variants of soft dynamics can be envisioned, but none can be rigorously defended from fundamental QCD. One of the attractive aspects of going to the highest possible collider energies is that the theoretical uncertainties due to soft dynamics are reduced, as more and more of the dynamics becomes dominated by calculable semi-hard and hard QCD processes.

2.4 Minijets and Transverse Flow

To summarize the consistency of HIJING calculations with the available experimental data, I show in Fig. 3 the inclusive spectra of charged particles in pp and $p\bar{p}$ over a wide energy range, $\sqrt{s}$ =50–1800 GeV. We see that the model accounts well for the energy dependence of not only the transverse momentum distribution, but also the rapidity distribution, as well as the multiparticle fluctuations. This overall quantitative understanding of multiparticle observables in hadronic interactions, especially the magnitude and energy dependence of the conspicuous power-law tail of the p_T spec-

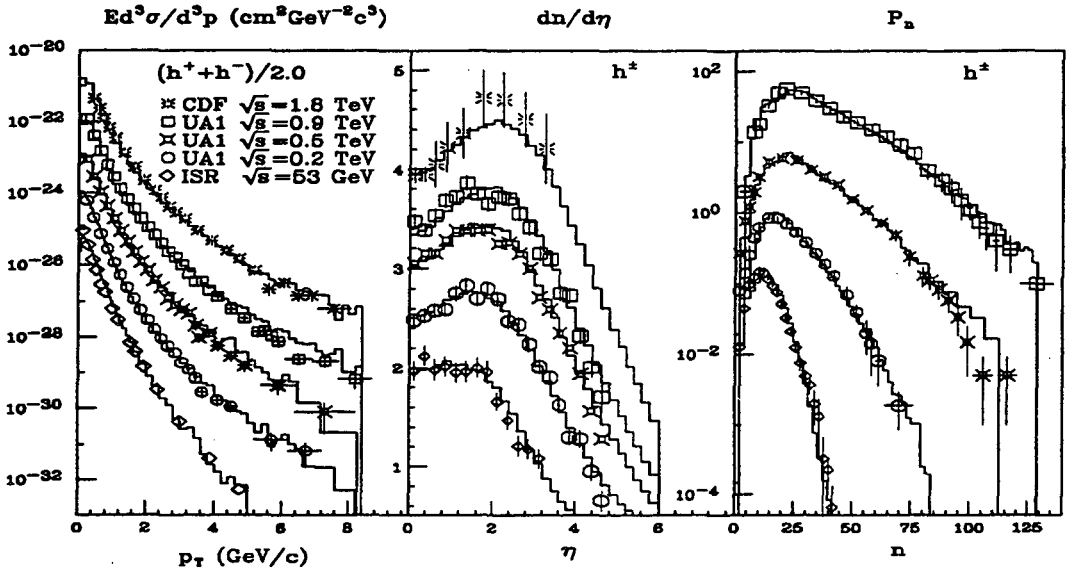

Figure 3: Data on charged particle inclusive p_T spectra $Ed^3\sigma/d^3p$ [64, 65, 66], pseudorapidity distributions $dn/d\eta$ [67, 68], and multiplicity distributions [69, 70, 71] P_n in pp and $p\bar{p}$ collisions compared to HIJING calculations at different energies $\sqrt{s}$. The transverse momentum spectra and multiplicity distributions have been displaced for clarity by extra factors of 10 relative to the absolutely normalized data at $\sqrt{s} = 53$ GeV.

trum characteristic of pQCD, strongly supports the importance of minijets physics at collider energies. To demonstrate the onset of particle production with minijet production, I plot in Fig. 4 the energy dependence of the central rapidity density of produced charged particles. I also show the contribution from purely soft interactions. Since the central rapidity density from soft string fragmentations is almost constant as a function of the colliding energy, the increased $dn_{\rm ch}/d\eta$ mainly comes from the hadronization of jets at high energies. The correlation between the central rapidity density and minijets is very clear when $dn_{\rm ch}/d\eta$ is compared with the average number of minijets, $\langle n_{jet}\rangle = \sigma_{\rm jet}/\sigma_{\rm in}$, as functions of $\sqrt{s}$.

Beside providing overall agreement with experimental data on multiparticle distribution and spectra [17, 74], minijet production will also influence correlations between observed quantities, some of which could be mistakenly attributed to QGP and other collective phenomena. One typical example is the multiplicity and mass dependence of the average transverse momentum observed in $p\bar{p}$ collisions at Tevatron Collider energy [75]. In hydrodynamic models, transverse collective flow is usually generated from the expansion of the thermalized dense system [76]. Since all hadrons have the same flow velocity, heavy particles tend to have larger transverse momentum

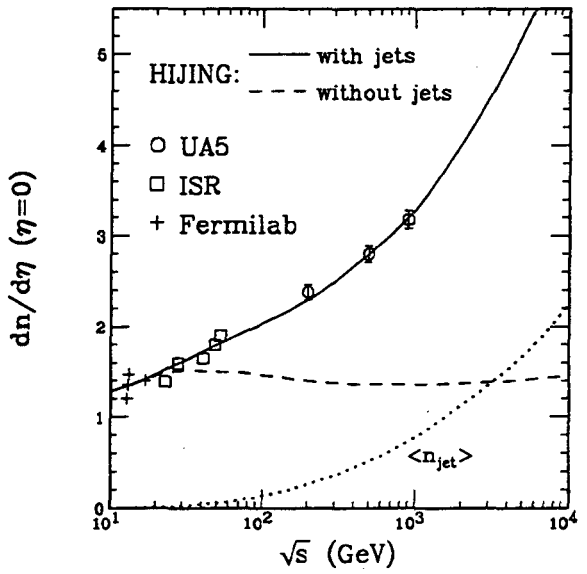

Figure 4: $dn_{\rm ch}/d\eta(\eta = 0)$ in inelastic pp and $p\bar{p}$ collisions as a function of $\sqrt{s}$. The solid line is the HIJING calculation compared to the data [67, 72, 73]. The dashed line is for events without jet production in HIJING simulations. The dotted line is the calculated average number of jets,$\langle n_{jet}\rangle = \sigma_{\rm jet}/\sigma_{\rm in}$.

when they finally freeze out. If the average transverse momentum is plotted against the total multiplicity, it is anticipated that for heavy particles it will be larger and the increase with the multiplicity will be faster than for light ones. Quite surprisingly, experiments on $p\bar{p}$ collisions at Tevatron Collider energy have recently reported observation of just this effect [75]. Lévai and Müller [77] have studied this reaction in a linearized transport theory. They found that there is no time for the baryons to equilibrate with the pions during the expansion of a hadronic fireball. They therefore suggested that a more novel explanation could be required to account for the apparent similarity of the flow velocities of the mesons and baryons. They noted that these observations could be understood if an equilibrated quark-gluon plasma (QGP) were formed in these collisions[78].

However, as also noted by Lévai and Müller, the common transverse flow of hadrons may also arise accidentally from the fragmentation of minijets. This is indeed what has been found with HIJING calculations [79]. Shown in Fig. 5 is the HIJING result of the correlation between $\langle p_T\rangle$ and the total charged multiplicity $n_{\rm ch}$ for pions, kaons, and antiprotons (from bottom to top) as solid lines together with the data at Tevatron energy. The average multiplicity density $\langle dn_{\rm ch}/d\eta\rangle$ is calculated as $n_{\rm ch}(|\eta| < \Delta\eta)$ divided by $2\Delta\eta$. The average p_T is obtained by applying the same procedure as used in the experiment [75] in which the p_T distributions are first fitted

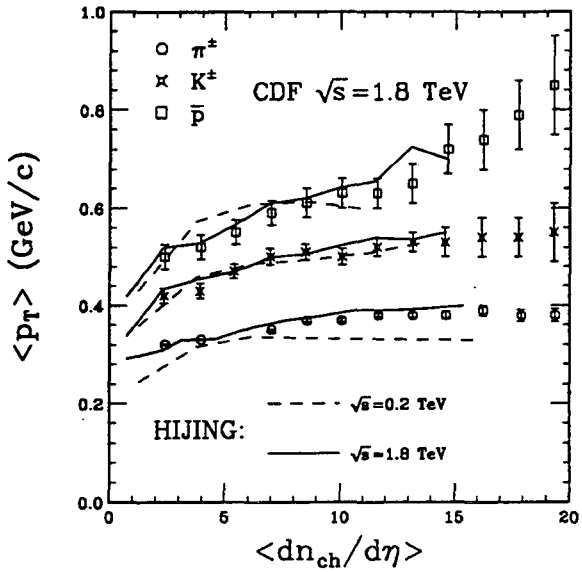

Figure 5: $\langle p_T \rangle$ of pions, kaons, and anti-protons (from bottom to top) in $-0.36 < \eta < 1.0$ versus the average charged multiplicity density $dn_{\rm ch}/d\eta$ in $|\eta| < 3.25$. The histograms are HIJING results and points are the data [75]. The dashed lines are for pp at $\sqrt{s} = 200$ GeV.

with parametrizations [power law $a(p_T + b)^{-n}$ for pions and exponential $\beta \exp(-\alpha p_T)$ for kaons and antiprotons] and then the fitted parameters are used to calculate $\langle p_T \rangle$ in the restricted range $0 < p_T < 1.5$ GeV/c. Apparently, the data are well accounted for by our calculation. Shown as dashed lines in Fig. 5 are the calculated results for pp collisions at RHIC energy, $\sqrt{s} = 200$ GeV. They are similar to the results at $\sqrt{s} = 1.8$ TeV, except that pions have a lower saturated value of $\langle p_T \rangle$ at RHIC energy. Since pions are the dominant produced particles, the high multiplicity $\langle p_T \rangle$ for all charged hadrons at $\sqrt{s} = 200$ GeV is smaller than at $\sqrt{s} = 1.8$ TeV.

In a model with multiple parton production, it is easy to understand why $\langle p_T \rangle$ increases with $n_{\rm ch}$. If we decompose the multiplicity distribution into different contributions from events with different number of minijets as shown in Fig. 6, we find that large multiplicity events are dominated by multiple minijet production while low multiplicity events are dominated by those of no jet production. The average transverse momentum in events with multiple minijets is certainly larger than those without, thus leading to the increase of $\langle p_T \rangle$ with $n_{\rm ch}$. In order to understand the different behavior of the correlations between $\langle p_T \rangle$ and $n_{\rm ch}$ for different particles, we recall that the jet fragmentation functions for heavy hadrons tend to be harder than for light hadrons, as measured in e^+e^- annihilation experiments[80]. Therefore, heavy hadrons from jet fragmentation carry larger transverse momenta than light hadrons in

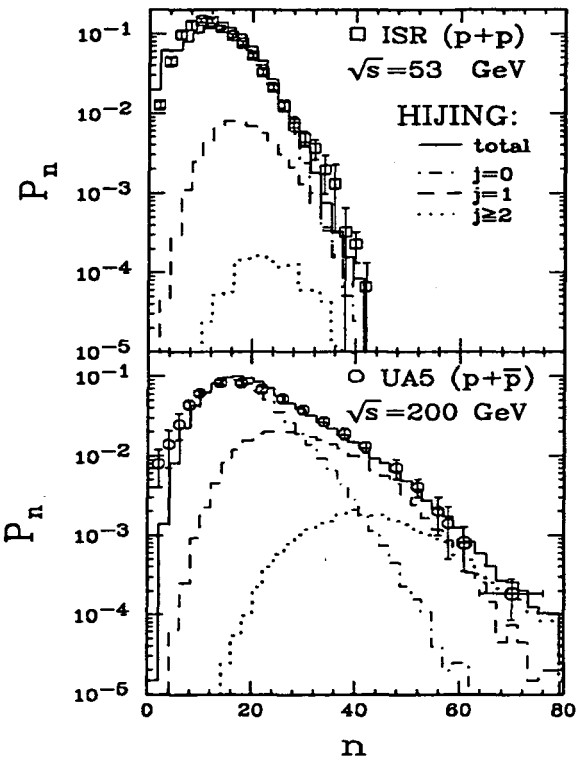

Figure 6: Charged multiplicity distributions in NSD pp at $\sqrt{s} = 53$ GeV and $p\bar{p}$ collisions at $\sqrt{s} = 200$ GeV. The data are from Refs. [69, 70]. The solid histograms are from the HIJING calculation with contributions from events with $j = 0$ (dot-dashed histograms), $j = 1$ (dashed histograms), and $j \geq 2$ (dotted histograms) jet production.

pp or $p\bar{p}$ collisions. This leads naturally to larger slopes of the $\langle p_T \rangle$ vs $n_{\rm ch}$ correlation for heavier particles. In other words, the fragmentation of minijets can mimic the transverse "flow" effect giving the resultant appearance of collective behavior.

Now one may ask: if totally different models [77, 81] can both describe the data, which one has the true underlying dynamics and how can they be distinguished from each other? To answer these questions, one has to turn to the properties of jet fragmentation.

2.5 Resolving Minijets in Hadronic Interactions

Jets in hadronic interactions, as defined earlier, are produced by large p_T parton scatterings in pQCD. Experimentally, jets are identified as hadronic clusters whose transverse energy E_T can be reconstructed from a calorimetrical study of the events [83]. However, this cluster-finding method becomes questionable for small and even

intermediate E_T values due to the background of fluctuations [84] from the underlying soft interactions. It has therefore been very difficult to resolve minijets with $p_T \gtrsim 2$ GeV/c from the underlying soft background.

Although minijets with $p_T \gtrsim 2$ GeV/c are difficult to resolve as distinct jets from the background, their effects even in minimum biased events, as we have demonstrated, can explain many aspects of hadronic collisions and the associated multiparticle production [33]. I have proposed [82] that the p_T dependence of the two-particle correlation function can be utilized to study the minijet content in the minimum biased events of hadronic interactions. Because particles from jet fragmentation tend to cluster in phase space, two-particle correlations must be enhanced due to minijet production. Especially for two-particle correlations in the azimuthal angle ϕ, contributions from back-to-back minijets should be strongly peaked in both forward ($\Delta\phi = 0$) and backward ($\Delta\phi = \pi$) directions. If we calculate the same correlations, but for some selected particles whose transverse momenta are larger than a certain p_T cut, the two peaks should be more prominent because these particles are more likely to come from minijets. On the other hand, particles from soft production or an expanding quark gluon plasma are isotropical in the transverse plane and would only have some nominal correlation in the backward direction due to momentum conservation. Therefore, the experimental measurement of two-particle correlation functions and their p_T dependence, especially in $p\bar{p}$ collisions at the Fermilab Tevatron energy where multiplicity and mass dependence of $\langle p_T \rangle$ were first observed, is essential to end the present controversy over whether the phenomenon is due to minijets, or string interaction [81] or the formation of a quark gluon plasma [77].

It is well known that particles from high p_T jets are very concentrated in both directions of the back-to-back jets. The widths of these high p_T jet profiles are about 1 in both pseudorapidity η and azimuthal angle ϕ [85]. Minijets, though with smaller p_T, should have similar properties. Since particles with $p_T > p_{T\text{cut}}$ are more likely to come from jet fragmentation, we can expect that the two-particle correlation functions are more characteristic of jet profiles when $p_{T\text{cut}}$ is larger. This method of two-particle correlations is unique because it can determine contributions to particle production from minijets which are intangible under the traditional cluster-finding algorithm [83] due to their small $p_T \sim 2$ GeV/c.

The normalized two-particle correlation functions in the azimuthal angle ϕ are defined as

$$c(\phi_1, \phi_2) = \frac{\rho(\phi_1, \phi_2)}{\rho(\phi_1)\rho(\phi_2)} - 1, \tag{38}$$

where $\rho(\phi)$ is the averaged particle density in ϕ and $\rho(\phi_1, \phi_2)$ is the two-particle density which is proportional to the probability of joint particle production at ϕ_1 and ϕ_2.

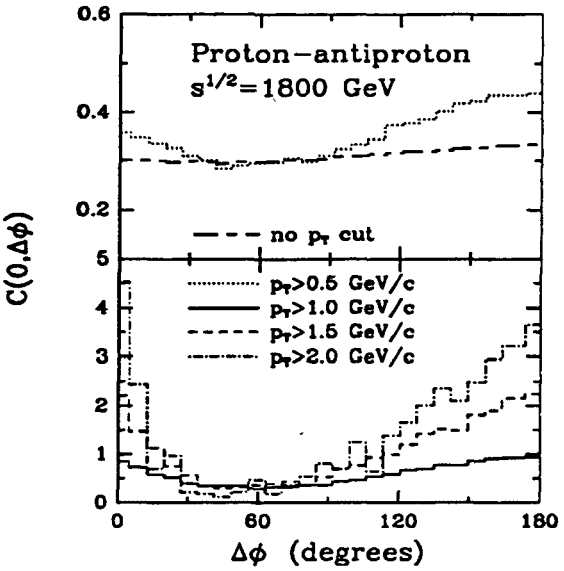

Figure 7: The correlation functions $c(0, \Delta\phi)$ vs $\Delta\phi$ between two charged particles in the full rapidity range in $p\bar{p}$ collisions at $\sqrt{s} = 1.8$ TeV. The dashed line is for all charged particles, dotted line for particles with $p_T > 0.5$ GeV/c, dash-dotted line for $p_T > 1.0$ GeV/c, and solid line for $p_T > 1.5$ GeV/c.

Shown in Fig. 7 are our calculated results on two-particle correlation functions in $p\bar{p}$ collisions at $\sqrt{s} = 1.8$ TeV for selected particles with different $p_{T\text{cut}}$. The calculation includes all charged particles in the full rapidity range. As we have expected, due to minijets, there is strong two-particle correlation at both $\Delta\phi = 0$ and π, forming a valley at $\Delta\phi \sim \pi/3$. For large $p_{T\text{cut}}$, the correlation functions are very similar to large p_T jet profiles as functions of ϕ relative to the triggered jet axis [85]. These features are, however, absent in low-energy hadronic collisions where minijet production is negligible [82]. Since there are still many particles from soft production which can contribute only to the backward correlation due to momentum conservation, the study of energy dependence of the relative heights of the two peaks at $\Delta\phi = 0$ and π could provide us information about the energy dependence of minijet production. The background at $\Delta\phi \sim \pi/3$ also depends on the average number of minijets produced[82].

Unlike high p_T back-to-back jets which are both kinematically bounded to the central rapidity region, a pair of minijets can be easily produced with a large rapidity gap between them. When we trigger one minijet in a limited rapidity window, the other one which is produced in the same parton scattering often falls outside the fixed rapidity window. Therefore, if we calculate two-particle correlations for particles in a limited rapidity range, the minijet contribution to the backward correlation ($\Delta\phi = \pi$)

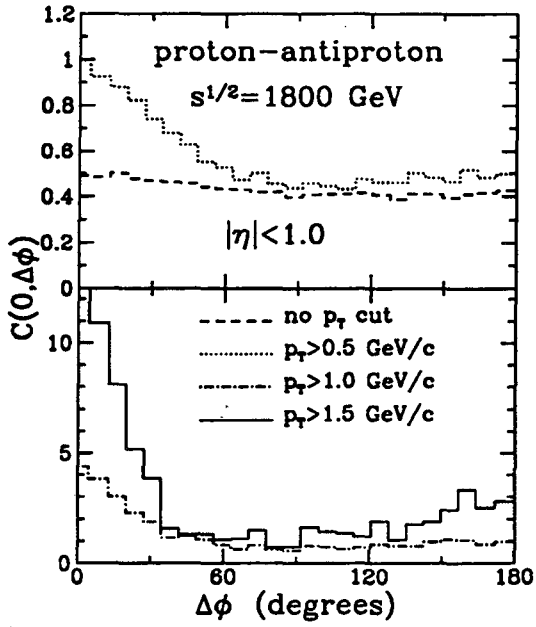

Figure 8: The same as Fig. 7, except for charged particles in a limited rapidity range of $|\eta| < 1$.

will mostly drop out while the contribution to forward correlation ($\Delta\phi = 0$) still remains. Indeed, as shown in Fig. 8, the forward correlation at $\Delta\phi = 0$ for particles in $|\eta| < 1$ is very strong, but the backward correlation at $\Delta\phi = \pi$ is drastically reduced as compared to the correlation pattern in the full rapidity range in Fig. 7. Furthermore, due to strong short range two-particle correlations in rapidity [74], the forward correlation at $\Delta\phi = 0$ is also enhanced by restricting particles to $|\eta| < 1$. At $\sqrt{s} = 1.8$ TeV, we find that the enhancement of backward correlation at $\Delta\phi = \pi$ due to minijets becomes important only when the rapidity window is $|\eta| \gtrsim 2$.

3 Parton Production in Nucleus-Nucleus Collisions

When we extrapolate the model to hadron-nucleus and nucleus-nucleus collisions, nuclear effects due to multiple parton scatterings and the interference have to be considered. Those nuclear effects can be generally divided into the two categories of initial and final state interactions. Initial state interactions and the interference lead to an apparent depletion of the effective parton density inside a nucleus, the so-called nuclear shadowing. They also lead to a modification of the momentum spectra of

produced partons, the Cronin effect [86], at intermediate energies. However, as I will demonstrate below, the Cronin effect will disappear at large transverse momentum and at high energies, like other high-twist processes. Both initial and final state scatterings can cause a fast parton to lose its energy. Due to color interference, this energy loss is not directly proportional [27, 31, 32] to the parton's energy. Thus for extremely energetic initial partons, this energy loss will be negligible. However, for produced partons which travel in the transverse direction, the energy loss becomes important relative to their finite transverse momentum. This energy loss will essentially modify the parton fragmentation, as well as accelerate parton equilibration.

3.1 Nuclear Shadowing of Parton Distribution Functions

Let us start first with the effect of nuclear modification of the parton distributions, or nuclear shadowing due to initial state interactions. What we are mostly concerned about here is the depletion of the effective parton density which will reduce the initial produced parton density and the transverse energy density[19, 87, 88]. This Section is based mainly on the work by Eskola, Qiu and myself in Ref. [100].

"Nuclear shadowing" in the context of the deeply inelastic lepton-nucleus scattering refers to the measured depletion of the nuclear structure function F_2^A at small $x_{\rm Bj}$, as compared to F_2 of unbound nucleons [89]. The same kind of depletion at small x is expected to happen also in the nuclear gluon distributions. During the recent years there have been many efforts to explain the measured nuclear shadowing of quarks and antiquarks [28, 90, 91, 92, 93, 94], but for gluons the situation is still inconclusive. In these models, shadowing at small x can be attributed to parton fusions before the hard scattering which probes the parton distributions. In terms of parton fusions, shadowing is also predicted to happen in protons. In this case, "shadowing" refers to the saturation of the actual parton distributions caused by fusions of overcrowding gluons at very small x. This mechanism proceeds through perturbative QCD-evolution as formulated in [37, 95]. It has been shown by Collins and Kwieciński that the singular gluon distributions actually saturate due to gluon fusions [96]. I will first review QCD-evolution of parton distributions and then demonstrate how parton shadowing arises from the inclusion of a fusion term in the evolution equation.

Parton distribution functions inside a nucleon or nucleus are closely related to the Pomeron substructure and its coupling to quarks and gluons [37, 46]. If one assumes that the ladder diagram inside a Pomeron is ordered in p_T, then one can derive a set of evolution equations for the parton distribution functions with respect

to the momentum scale of the hard scattering [42, 97]:

$$Q^2\frac{\partial q_i(x,Q^2)}{\partial Q^2} = \frac{\alpha_s(Q^2)}{2\pi}\int_x^1\frac{dy}{y}\left[P_{q\to qg}(y)q_i(\frac{x}{y},Q^2)+P_{g\to q\bar{q}}(y)g(\frac{x}{y},Q^2)\right], \quad (39)$$

$$Q^2\frac{\partial g(x,Q^2)}{\partial Q^2} = \frac{\alpha_s(Q^2)}{2\pi}\int_x^1\frac{dy}{y}\left[\sum_{i=1}^{2N_f}P_{q\to gq}(y)q_i(\frac{x}{y},Q^2)+P_{g\to gg}(y)g(\frac{x}{y},Q^2)\right] \quad (40)$$

where the splitting functions, $P_{a\to bc}(y)$, are the probability distribution functions for the respective radiative processes as illustrated in Fig. 9(a), x is the fractional momentum of the specified partons, and N_f is the number of quark flavors. In addition to these splitting processes, one should also take into account the virtual corrections as shown in Fig. 9(b). Their contributions to the evolution equations are [98]

$$q_i(x,Q^2): \quad -\frac{\alpha_s(Q^2)}{2\pi}q_i(x,Q^2)\int_0^1 dyP_{q\to qg}(y), \quad (41)$$

$$g(x,Q^2): \quad -\frac{\alpha_s(Q^2)}{2\pi}g(x,Q^2)\int_0^1 dy\frac{1}{2}\left[P_{g\to gg}(y)+N_fP_{g\to q\bar{q}}(y)\right]. \quad (42)$$

These virtual corrections are important to regularize the soft divergences in the splitting functions and guarantee flavor and momentum conservation. If one wants a probabilistic interpretation of the evolution and especially a numerical simulation, the above virtual corrections will give rise to the Sudakov form factors which are necessary to guarantee unitarity. As one can see, the above virtual corrections can be incorporated into the evolution equations by introducing a δ-function and "+functions" (see [97] for their definitions) in the splitting functions

$$P_{g\to q\bar{q}}(y) = \frac{1}{2}[y^2+(1-y)^2]; \quad (43)$$

$$P_{q\to gq}(y) = \frac{4}{3}\frac{1+(1-y)^2}{y}; \quad (44)$$

$$P_{q\to qg}(y) = \frac{4}{3}\left[\frac{1+y^2}{(1-y)_+}+\frac{3}{2}\delta(1-y)\right]; \quad (45)$$

$$P_{g\to gg}(y) = 6\left[\frac{y}{(1-y)_+}+\frac{1-y}{y}+y(1-y)+\frac{1}{12}(11-\frac{2}{3}N_f)\delta(1-y)\right]. \quad (46)$$

With the above splitting functions one can check that flavor and momentum are

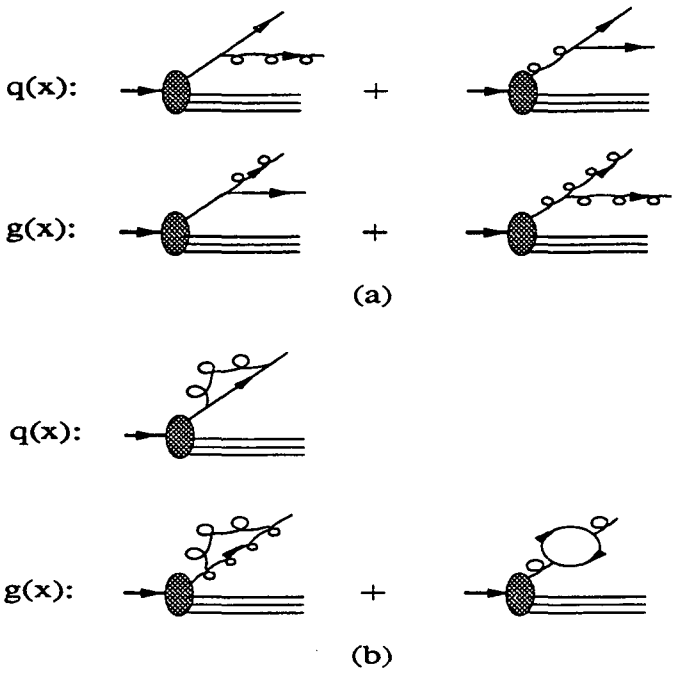

Figure 9: (a) Radiative and (b) virtual corrections to parton distributions.

conserved, *i.e.*,

$$\frac{\partial}{\partial Q^2}\int_0^1 dx\left[q_i(x.Q^2)-\bar{q}_i(x,Q^2)\right] = 0, \tag{47}$$

$$\frac{\partial}{\partial Q^2}\int_0^1 dx x\left[g(x,Q^2)+\sum_{i=1}^{2N_f} q_i(x,Q^2)\right] = 0. \tag{48}$$

In the parton model, a nucleus consists of many valence quarks. Those valence quarks, however, are dressed with clouds of sea quarks and gluons due to vacuum fluctuations (which corresponds to the loops inside a Pomeron ladder). The life time of the virtual partons is of the order of the hadron size, $R_N \sim 1$ fm. If those valence quarks are probed by a hard scattering with resolution $Q \gg 1/R_N$, the coherence of the parton clouds will be broken and numerous partons will be released. The parton density inside the clouds will then depend on the resolution of the scattering Q. The larger the Q the denser the parton clouds, as predicted by the QCD evolution equations. These evolution equations are based on perturbative QCD which can only be applied down to some scale Q_0. Given the initial values of parton distributions at Q_0, the evolution in $Q > Q_0$ can be predicted by pQCD. However, the parton distributions below Q_0 cannot be obtained from pQCD and so far can only be determined from experiments.

At small values of x, the leading order QCD evolution equations predict that the number of gluons becomes extremely large. It has been known [37, 95] that for sufficiently small values of x and/or of Q^2, the total transverse area occupied by the gluons will be larger than the transverse area of a hadron, so that the interactions among gluons can no longer be neglected. Such gluon recombination results in a modification of the QCD evolution equations, Eqs. (39) and (40). In the limit of small-x and neglecting quark distributions, the modified QCD evolution equation for the gluon distribution can be cast in the form [37, 95]

$$\partial_y \partial_t G(y,t) = cG(y,t) - \gamma \exp(-t - e^t)[G(y,t)]^2, \tag{49}$$

where $y = \ln(1/x)$, $t = \ln[\ln(Q^2/\Lambda^2_{\rm QCD})]$, $G(y,t) = xg(x,Q^2)$ and $c = 12/(11-2N_f/3)$ with N_f the number of quark flavors.

The seond term in Eq. (49) corresponds to the change of the distribution due to gluon recombination. The strength of the gluon recombination is controlled by the factor γ, originating from two possible sources. One can consider gluon fusion in terms of one Pomeron to two-Pomeron coupling. The two fusing gluon ladders (two Pomerons), which couple 4 gluons to 2 gluons, can arise either from independent constituents of the proton/nucleus or from the same one, as discussed in [95, 96, 99]. We will refer to the former case as "independent" and to the latter as "non-independent" fusion. Since recombinations from both sources happen simultaneously, we divide the parameter γ into two parts:

$$\gamma = \gamma_{\rm I} + \gamma_{\rm II}, \tag{50}$$

where $\gamma_{\rm I}$ corresponds to the independent recombination and $\gamma_{\rm II}$ to the non-independent one.

To understand the form of the fusion term in Eq. (49), one can consider $xg(x,Q^2)$ as the gluon number n_g per unit rapidity ($dy = dx/x$). If we note that the gluon-gluon cross section $\hat{\sigma} \sim \alpha_s/\Lambda^2_{\rm QCD}$, the independent gluon fusion probability inside a nucleon with transverse area πR_N^2 is then,

$$W = \frac{n_g^2 \hat{\sigma}}{\pi R_N^2} \sim \frac{\alpha_s}{R_N^2 \Lambda^2_{\rm QCD}} [xg(x,Q^2)]^2. \tag{51}$$

This corresponds to the gluon fusion term in Eq. (49) (note that $e^{-t} \sim \alpha_s$). One can calculate this fusion term in a QCD recombination model [95]. In a proton, the

strength of the independent fusion then takes the form

$$\gamma_{\rm I} = \frac{2}{3}\frac{1}{\pi R_N^2}\cdot\frac{\pi^3 c^2}{2\Lambda_{\rm QCD}^2}, \tag{52}$$

where $R_N \sim 1$ fm is the radius of a proton.

The non-independent fusion happens inside the same valence quark which is assumed to have a transverse size $\sim 1/Q_i$. The magnitude of the non-independent fusion of the gluon ladders can be estimated as [95]

$$\gamma_{\rm II} \approx \frac{16}{81}\frac{1}{\pi(2/Q_i)^2}\cdot\frac{\pi^3 c^2}{2\Lambda_{\rm QCD}^2}, \tag{53}$$

where a simplification is made by fixing the initial x of the valence quark to $x_i \sim 1$. We also approximate the scale of the initial valence quark by $Q_i \sim 2$ GeV.

Let us then consider a large loosely bound nucleus. Naturally, both types of fusions are still there but only for the independent one an $A^{1/3}$-scaling arises. In this case

$$\gamma_{\rm I}^A = \frac{9}{8}\frac{A}{\pi R_A^2}\cdot\frac{\pi^3 c^2}{2\Lambda_{\rm QCD}^2}, \tag{54}$$

where the nucleus is taken to be a sphere with a sharp surface at $R_A = 1.12A^{1/3}$ fm. The strength of the non-independent fusion remains the same as in the case of a free proton: $\gamma_{\rm II}^A = \gamma_{\rm II}$.

It is interesting to notice how the relative contributions of the two types of recombination will change when going from a proton to a nucleus of $A \sim 200$: $\gamma_{\rm II}/\gamma_{\rm I} \approx 7.6$ and $\gamma_{\rm II}^A/\gamma_{\rm I}^A \approx 1.0$. Thus the non-independent fusion is clearly dominant in a free proton while in a large nucleus the contributions from both types are of the same order. As a result, parton recombination is strongly enhanced in a heavy nucleus.

In order to solve Eq. (49) exactly by integration, one would need the initial distribution either at fixed y_0 or t_0 *and* the derivatives along a boundary line (y, t_0) or (y_0, t), respectively. However, since the expression for the non-linear term in Eq. (49) is not valid for the regions where x is large, or where both x and Q are very small, the natural boundary condition at $x = 1$ (or $y_0 = 0$) is not suitable here. In addition, since we do not have sufficient information on other boundary lines, we cannot solve Eq. (49) by direct integration. Instead, with the semiclassical approximation [37], we use the method of characteristics [96, 100], so that we can avoid the region of both small x and small Q^2.

The semiclassical approximation corresponds to neglecting the second order

derivative term, $\partial_y \partial_t \ln(G)$, which leaves us with the evolution equation as

$$\partial_y z(y,t) \partial_t z(y,t) = c - \gamma \exp[-t - e^t + z(y,t)], \tag{55}$$

where $z(y,t) = \ln[G(y,t)]$. The reason why this approximation is called semiclassical is that it corresponds to using a saddle-point approximation to the integration in the integral form of the evolution equation. The above equation can then be cast and solved in the form of a set of characteristic equations as shown in detail in [96]. What is needed here is the gluon distribution at the boundary $y_0[= -\ln(x_0)]$ at all t, which can be obtained by evolving the distribution in the region $x > x_0$ according to the original GLAP evolution equations, Eqs. (39) and (40).

For a proton, we assume that the recombination becomes effective at $x \sim x_0 \sim 0.01$, which is consistent with [96, 99]. We can use the results from a global fitting to the parton distributions, like CTEQ [101], to constrain x_0. In fact, we will see that with $x_0 = 0.01$ the shadowed gluons deviate considerably from the CTEQ gluons only after $x < 0.001$, so our choice for x_0 seems to be reasonable, and we do not expect the results to be very sensitive to small changes of x_0.

As explained above, the gluon recombination is strongly enhanced in heavy nuclei and it starts at somewhat larger values of x than in protons. The corresponding boundary line x_0^A for a nucleus is approximately determined by the relative magnitude of the evolution terms in Eq. (49): for $G_A(x_0^A) \sim G(x_0)\gamma_A/\gamma$, the relative contribution from the gluon fusion in a nucleus is about the same as in a nucleon. This gives $x_0^A \sim 0.05$–0.1. This range of x_0^A is also supported by other studies [102].

Let the total gluonic fractional momentum in the non-shadowed parton distributions be $f_0 = \int_0^1 dx\, x g_{\rm CTEQ}(x, Q_0^2)$. In the case of a proton, shadowing changes the gluonic momentum typically by less than a per cent, which we can clearly neglect as a small overall change.

Perturbative shadowing at small x reduces the gluonic momentum more in a nucleus than in a proton. If the momentum fraction of gluons is conserved, there must be a corresponding enhancement in the large x region. However, there can also be momentum transfers from quarks and antiquarks to the gluons. Here we consider nuclei with $A \sim 200$, for which we expect an overall increase in the gluonic momentum fraction, ϵ_A, to be only about 4% [91, 92, 102] as constrained by the experimental data on quark (anti-quark) shadowing in deep inelastic scatterings. These two sources of momentum flow will result in anti-shadowing (enhancement of parton densities) at large $x > x_0^A$. To account for the anti-shadowing we assume $g(x, Q_0^2) = a_A g_{\rm CTEQ}(x, Q_0^2)$ for $x > x_0^A$ with $g_{\rm CTEQ}(x, Q_0^2)$ the non-shadowed gluon

distribution and $a_A > 1$ to be determined by the momentum sum rule,

$$\int_0^{x_0^A} dx\, x g(x,Q_0^2)\Big|_C \;+\; a_A \int_{x_0^A}^1 dx\, x g_{\rm CTEQ}(x,Q_0^2) = f_0(1+\epsilon_A). \qquad (56)$$

The right-hand-side of the equation is the gluonic momentum fraction of the non-shadowed parton distributions plus the momentum transfer ϵ_A from quarks and anti-quarks during the recombination. One can solve the above equation iteratively for a_A with the boundary condition $C: g_A(x_0^A,Q_0^2) = a_A g_{\rm CTEQ}(x_0^A,Q_0^2)$. Typically, $a_A \sim 1.1$ for $A \sim 200$.

In Fig. 10(a), nucleon and effective nuclear gluon distributions for a nucleus of $A = 200$ are compared with the input CTEQ gluon distribution at $Q_0 = 2$ GeV. Notice the ~20 % uncertainty in the nuclear case resulting from varying x_0^A from 0.05 to 0.1. To demonstrate the formation of strong perturbative nuclear shadowing, corresponding to the *relative* depletion of gluon distributions in a nucleus, we plot the ratio $G_A(x,Q_0^2)/G(x,Q_0^2)$ in Fig. 10(b). Notice also that as x decreases, the gluon distribution in a proton increases much faster, or approaches saturation at a much smaller x than that in a nucleus. Therefore, as shown in Fig. 10(b) the ratio saturates only when the gluons in a *proton* do so. Thus, saturation of the perturbative nuclear shadowing reflects actually the behavior of the gluons in a proton. We see that, due to the enhanced gluon recombination in a heavy nucleus, a ~50% nuclear shadowing in small-x region is generated perturbatively through the modified QCD evolution, accompanied by a ~10 % antishadowing from momentum conservation.

We have not included the non-perturbative, *e.g.*, Glauber-derived [28] contribution to the shadowing. Inclusion of such a contribution is equivalent to changing the initial values of gluon distribution at scale Q_0 and will slightly reduce the perturbative contribution to the shadowing through QCD evolution. We also have not considered the shadowing of quark distributions in this study of perturbative shadowing. However, experimental data [89] on quark shadowing are roughly consistent with the perturbative gluon shadowing we have just estimated. The shadowing, at least for quarks, has been shown to depend weakly on the scale Q [102], also consistent with experimental data.

For a practical implementation of the nuclear shadowing in HIJING, we consider that quarks and gluons are shadowed by the same amount inside a nucleus and use the following parametrized form:

$$R_A(x) \;\equiv\; \frac{f_{a/A}(x)}{A f_{a/N}(x)}$$

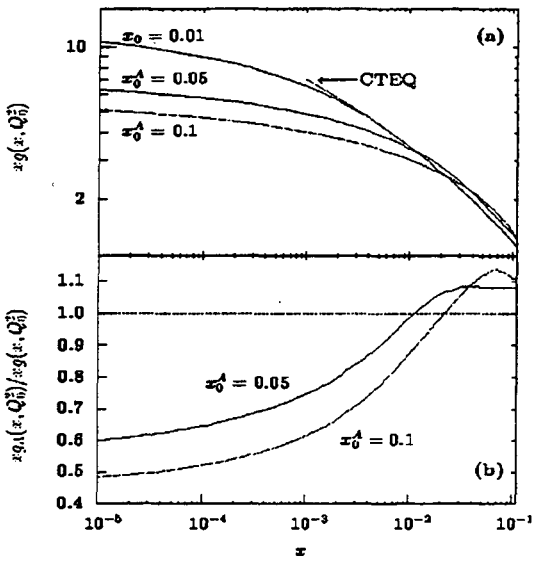

Figure 10: (a) The gluon distributions $xg(x,Q_0^2)$ at $Q_0 = 2$ GeV vs. x. The result for proton is labeled by x_0, and the results for $A \sim 200$ by x_0^A, respectively. The CTEQ gluon distribution [101] is labeled by "CTEQ". (b) The ratio $xg_A(x,Q_0^2)/xg(x,Q_0^2)$ of the shadowed gluon distributions vs. x, demonstrating a strong perturbative nuclear shadowing in heavy nuclei.

$$= 1 + 1.19\ln^{1/6}A\,[x^3 - 1.5(x_0+x_L)x^2 + 3x_0x_Lx] - \left[\alpha_A - \frac{1.08(A^{1/3}-1)}{\ln(A+1)}\sqrt{x}\right] e^{-x^2/x_0^2}, \quad (57)$$

$$\alpha_A = 0.1(A^{1/3}-1), \quad (58)$$

where $x_0 = 0.1$ and $x_L = 0.7$. The term proportional to α_A in Eq. (57) determines the shadowing for $x < x_0$ with the most important nuclear dependence, while the rest gives the overall nuclear effect on the structure function in $x > x_0$ with a very weak A dependence. As shown in Fig. 11 , this parametrization reproduces the measured overall nuclear effect on the quark structure function in the small and medium x regions. However, I should emphasize that this parametrization does not satisfy the momentum sum rule and does not include the weak scale dependence which was found by Eskola in a detailed study in Ref. [102].

Eq. (57) represents only the average nuclear dependence of the structure function. However, in pA or AA collisions, we have to calculate the effective jet cross sections at the nucleon-nucleon level for each impact parameter. Physically, it is natural to expect that the nuclear effects on the structure functions could depend on the local nuclear thickness at each impact parameter [87]. Eq. (58) is consistent with the

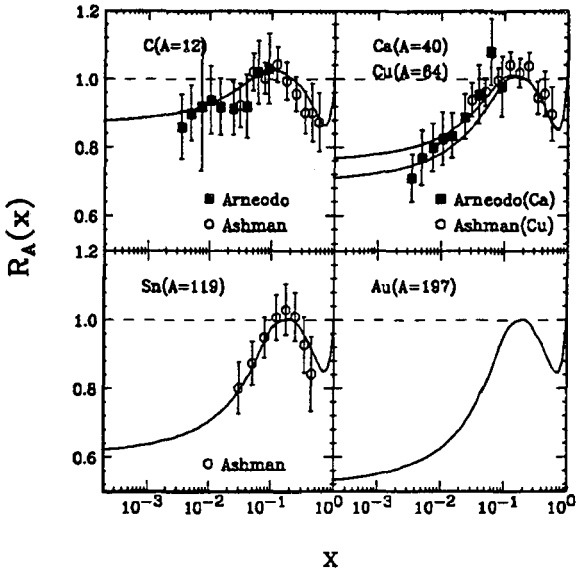

Figure 11: The ratio of quark structure functions $R_A(x) \equiv F_2^A(x)/AF_2^N(x)$ as a function of x in small and medium x regions for different nuclear mass numbers A. The data are from Ref. [89] and curves are the parametrization in Eqs. (57) and (58).

assumption that the shadowing parameter $\alpha_A(r)$ is proportional to the longitudinal thickness of the nucleus at impact parameter r. We therefore parameterize the impact parameter dependence of α_A in Eq. (57) as

$$\alpha_A(r) = 0.1(A^{1/3} - 1)\frac{4}{3}\sqrt{1 - r^2/R_A^2}, \tag{59}$$

where r is the transverse distance of the interacting nucleon from its nucleus center and R_A is the radius of the nucleus. For a sharp-sphere nucleus with thickness function $T_A(r) = \frac{3A}{2\pi R_A^2}\sqrt{1 - r^2/R_A^2}$, the averaged $\alpha_A(r)$ is $\int_0^{R_A^2} \pi dr^2 T_A(r)\alpha_A(r)/A = \alpha_A$, with α_A from Eq. (58). Because the rest of Eq. (57) has a weaker A dependence, we only consider the impact parameter dependence of α_A.

To simplify the calculation during the Monte Carlo simulations, we can decompose $R_A(x,r)$ into two parts,

$$R_A(x,r) \equiv R_A^0(x) - \alpha_A(r)R_A^s(x), \tag{60}$$

where $\alpha_A(r)R_A^s(x)$ is the term proportional to $\alpha_A(r)$ in Eq. (57) with $\alpha_A(r)$ given in Eq. (59) and $R_A^0(x)$ is the rest of $R_A(x,r)$. Both $R_A^0(x)$ and $R_A^s(x)$ are now independent of r. The effective jet production cross section of a binary nucleon-

nucleon interaction in $A+B$ nuclear collisions can therefore be decomposed as [87]

$$\sigma_{\rm jet}^{eff}(r_A,r_B)=\sigma_{\rm jet}^0-\alpha_A(r_A)\sigma_{\rm jet}^A-\alpha_B(r_B)\sigma_{\rm jet}^B+\alpha_A(r_A)\alpha_B(r_B)\sigma_{\rm jet}^{AB}, \qquad (61)$$

where $\sigma_{\rm jet}^0$, $\sigma_{\rm jet}^A$, $\sigma_{\rm jet}^B$ and $\sigma_{\rm jet}^{AB}$ can be calculated through Eq. (19) by multiplying $f_a(x_1,p_T^2)f_b(x_2,p_T^2)$ in the integrand with $R_A^0(x_1)R_B^0(x_2)$, $R_A^s(x_1)R_B^0(x_2)$, $R_A^0(x_1)R_B^s(x_2)$ and $R_A^s(x_1)R_B^s(x_2)$, respectively.

In central $Au+Au$ collisions at $\sqrt{s}=200$ AGeV, the average parton fractional momentum is $x=2p_T/\sqrt{s}\simeq 0.02$ for mini-jets with $p_T\geq p_0=2$ GeV. The impact-parameter dependent parton shadowing reduces the averaged inclusive mini-jet cross section by 50% from its value in pp. This estimate will be somewhat modified if one includes the scale dependence of the shadowing effect. However, at RHIC energies we can see from Fig. 11 that mini-jet production with $x\simeq 0.02$ is still not in the deep-shadowed region of x. For sufficiently high energies, most of the mini-jets come from $x\lesssim 0.01$ region so that the effective mini-jet cross section may be reduced by a factor 3 in central $Au+Au$ collisions. Note that this large reduction of mini-jet multiplicity by gluon shadowing may increase the limit for independent multi-jet production up to $\sqrt{s}=50$ ATeV for $Au+Au$ collisions.

3.2 Disappearance of Cronin Effect at High Energies

In hadron-nucleus and nucleus-nucleus collisions, multiple scatterings happen both at hadronic and partonic levels. Due to the interference between multiple scattering amplitudes, a hadron can only "see" the surface of a nucleus, leading to a total cross section $\sim R_A^2$. Parton fusions which cause nuclear shadowing of the parton distribution functions can also be viewed as multiple parton scattering in the laboratory frame. The parton depletion arises from the destructive interference among different scattering amplitudes [28]. These multiple scatterings and their interference will also affect the momentum spectra of the produced partons. In general, as observed first by Cronin *et al.* [86], particle production at large p_T will be enhanced. However, recent experiments [103] show that the enhancement decreases both with p_T and energy $\sqrt{s}$.

I would like to emphasize that the initial multiple scatterings discussed here are very different from the late final parton rescatterings which are responsible for parton thermalization. The initial partons in general have very small transverse momenta but large center-of-mass (c.m.) energies. As demonstrated in Ref. [27], multiple scatterings among these initial partons cannot be treated as semiclassical cascades which might be valid for final parton rescatterings. The eikonal limit is more relevant for the initial partons scatterings which can be treated by a Glauber multiple scattering analysis.

Following the same procedure that leads to the hadron-hadron scattering cross section due to exchange of multiple Pomerons, Eq. (14), one can also obtain the inelastic cross section for pA collisions,

$$\sigma_{pA}(s) = \int d^2b[1 - e^{-\sigma_{NN}(s)T_A(b,s)}], \tag{62}$$

where σ_{NN} is the total nucleon-nucleon cross section and

$$T_A(b) = \int_{-\infty}^{\infty} dz\rho(b,z), \tag{63}$$

is the thickness function of the nucleus at impact parameter b. The nuclear density, $\rho(b,z)$, is normalized to $\int d^2bT_A(b) = A$.

Let us assume that the total nucleon-nucleon cross section can be described by parton scatterings with given cross sections. Define the differential cross section for a parton-nucleon scattering, $i + N \to j + X$, as $h^{ij}(p_i, p_j)$, with the total cross section

$$\sigma_i(p_i) = \frac{1}{2}\sum_j \frac{d^3p_j}{E_j} h^{ij}(p_i, p_j). \tag{64}$$

Let us also define

$$T_A^{\pm}(b,z) = \pm \int_z^{\pm\infty} dz'\rho(b,z'). \tag{65}$$

Note that

$$T_A(b) = T_A^-(b,z) + T_A^+(b,z). \tag{66}$$

Now according to a Glauber multiple scattering interpretation of the pA cross section Eq. (62), the probabilities for parton i not to interact with the nucleons up to z and for j not to interact after z, are respectively,

$$e^{-\sigma_i(p_i)T_A^-(b,z)}, \quad e^{-\sigma_j(p_j)T_A^+(b,z)}. \tag{67}$$

Then, the probability for one parton-nucleon scattering, $i + A \to j + X$, is

$$\begin{aligned} \frac{dH_{(1)}^{ij}}{d^2b} &= \int_{-\infty}^{\infty} dz e^{-\sigma_i T_A^-(b,z)}\rho(b,z)h^{ij}e^{-\sigma_j T_A^+(b,z)} \\ &= \frac{h^{ij}}{\sigma_j - \sigma_i}\left[e^{-\sigma_i T_A(b)} - e^{-\sigma_j T_A(b)}\right] \\ &= h^{ij}T_A(b)\left[1 - \frac{\sigma_i + \sigma_j}{2}T_A(b)\right] + \cdots , \end{aligned} \tag{68}$$

where the definition of the thickness functions $T_A(b)$ and Eq. (66) have been used, and an expansion in terms of $\sigma_{i,j}T_A(b)$ has been made in the last step.

We can use the above result to calculate the probability for a parton k to have only one scattering after z, by replacing $T_A(b)$ with $T_A^+(b,z)$. Then the contribution to $i+A\to j+X$ from two parton-nucleon scatterings is

$$\begin{aligned}\frac{dH_{(2)}^{ij}}{d^2b} &= \sum_k \int_{-\infty}^{\infty} dz e^{-\sigma_i T_A^-(b,z)}\rho(b,z)\frac{h^{ik}h^{kj}}{\sigma_j-\sigma_k}\left[e^{-\sigma_k T_A^+(b,z)}-e^{-\sigma_j T_A^+(b,z)}\right]\frac{d^3p_k}{E_k}\\ &= \sum_k \frac{d^3p_k}{E_k}\frac{h^{ik}h^{kj}}{\sigma_j-\sigma_k}\left[\frac{e^{-\sigma_i T_A(b)}-e^{-\sigma_k T_A(b)}}{\sigma_k-\sigma_i}-\frac{e^{-\sigma_i T_A(b)}-e^{-\sigma_j T_A(b)}}{\sigma_j-\sigma_i}\right]\\ &= \frac{1}{2}T_A^2(b)\sum_k \frac{d^3p_k}{E_k}h^{ik}h^{kj}+\cdots\quad . \end{aligned} \tag{69}$$

Therefore, up to second order in $\sigma T_A(b)$, we have the cross section for $i+A\to j+X$,

$$\frac{dH^{ij}}{d^2b}\approx h^{ij}T_A(b)+\frac{1}{2}T_A^2(b)\left[\sum_k \frac{d^3p_k}{E_k}h^{ik}h^{kj}-(\sigma_i+\sigma_j)h^{ij}\right]. \tag{70}$$

In the second term in the above equation, we can already see that the interference between double and single scattering comes into play. If we assume the parton distribution inside the projectile nucleon to be $f_{i/N}(p_i)$, then the differential cross section for $N+N\to j+X$ is given by

$$\sigma_{NN}^j \equiv \sum_i \int \frac{d^3p_i}{E_i}f_{i/N}(p_i)h^{ij}. \tag{71}$$

Assuming a hard sphere for the nuclear density $\rho(r)$ with a radius $R_A=R_0A^{1/3}$, we then obtain the ratio between the differential cross sections of $N+A\to j+X$ and $N+N\to j+X$,

$$R_A\equiv\frac{\sigma_{NA}^j}{A\sigma_{NN}^j}=1+\frac{9A^{1/3}}{16\pi R_0^2}\frac{1}{\sigma_{NN}^j}\sum_i\int\frac{d^3p_i}{E_i}f_{i/N}(p_i)\left[\sum_k\frac{d^3p_k}{E_k}h^{ik}h^{kj}-(\sigma_i+\sigma_j)h^{ij}\right]. \tag{72}$$

Compared to the additive model of hard scatterings, parton production in NA collisions is enhanced due to multiple scattering. The enhancement is proportional to $A^{1/3}$, which is the average number of nucleons inside a nucleus along the beam direction. This formula was used successfully [104] to explain the enhancement of large p_T particle production in pA collisions.

To demonstrate how this enhancement depends on the transverse momentum and colliding energy, let us assume a simple power-law form for the parton-nucleon

differential cross section,

$$h^{ij} \equiv d\sigma/dydp_T^2 = C/p_T^n, \quad (|y| < \Delta Y/2, p_T > p_0). \tag{73}$$

Assuming that all partons are identical, the total cross section is then,

$$\sigma = \frac{1}{2}\int dyd^2p_T \frac{C}{p_T^n} = \frac{\pi \Delta Y C}{(n-2)p_0^{n-2}}. \tag{74}$$

For large $p_T \gg p_0$, one can evaluate the integral,

$$\begin{aligned}\int \frac{d^3p_k}{E_k} h^{ik}h^{kj} &= \int dyd^2q_T \frac{C}{q_T^n}\frac{C}{(\mathbf{p}_T - \mathbf{q}_T)^n} \\ &= \frac{C}{p_T^n}\sigma\left[2 + \frac{n(n-2)}{2}(p_0/p_T)^2 + \mathcal{O}((p_0/p_T)^4)\right].\end{aligned} \tag{75}$$

Substituting the above cross sections into Eq. (72), we have,

$$R_A = 1 + \frac{9A^{1/3}}{16\pi R_0^2}\sigma\frac{n(n-2)}{2}(p_0/p_T)^2 + \mathcal{O}((p_0/p_T)^4) \tag{76}$$

There are a few interesting features in the above estimate. The nuclear enhancement of jet cross sections decreases with p_T, a general feature of high-twist processes. It also depends on the power n of the differential parton cross section. This feature is a direct consequence of the interference effect, *i.e.*, the cancellation between terms in the single and double scattering amplitudes. From both pQCD calculations and experimental data, we know that the power n decreases with the colliding energy. Thus, the nuclear enhancement of large p_T parton production will decrease, and eventually it will disappear at high energies. This trend has already been observed in experiments [103] in the energy range $\sqrt{s} = 20 - 40$ GeV. A simple way to understand this energy dependence is the following. At low energies, the differential cross section for a single hard scattering decreases very fast with p_T (large power). It is then easier for the incident parton to acquire a large p_T through two successive scatterings, each with small transverse momentum transfer, than through a single large p_T scattering. This is why multiple scatterings in pA collisions cause the enhancement of large p_T parton production. As energy increases, the differential cross section for a single scattering decreases less rapidly with p_T as compared to low energies. It is no longer more economical to produce a large p_T parton through double scatterings than through a single scattering. At extremely high energies, the Cronin effect will disappear. Therefore, we will not consider multiple initial scatterings in the

following since we only consider parton production in heavy-ion collisions at future collider energies (RHIC and LHC).

3.3 Monte Carlo Simulations

Since we have argued that multiple initial parton scatterings will become unimportant at high energies, we can assume a binary approximation for hard scatterings. In that case, multiple hard processes involve only independent pairs of partons. Only very rarely does a given parton suffer two high p_T scatterings in one event. As the energy increases the number of partons that can participate in moderate $p_T > p_0$ processes increases rapidly and the nuclear shadowing phenomenon will also become important at small x. However, for the bulk of parton and transverse energy production, the basic independent binary nature of the multiple mini-jet production rate is expected to remain a good approximation as long as Eq. (26) holds.

For soft interactions, a nucleus-nucleus collision is also decomposed into binary collisions involving in general excited or wounded nucleons. Wounded nucleons are assumed to be $q - qq$ string-like configurations that decay on a slow time scale compared to the overlapping time of the nuclei. In the FRITIOF [13] scheme wounded nucleon interactions follow the same excitation law as the original hadrons. In the DPM [14] scheme subsequent collisions essentially differ from the first since they are assumed to involve sea partons instead of valence ones. In HIJING [19] we adopted a hybrid scheme, iterating string-string collisions as in FRITIOF but utilizing DPM-like distributions as in Eqs. (36) and (37). Another difference in the way soft interactions are treated in HIJING is that string-string interactions are also allowed to de-excite as well as to excite the strings further within the kinematic limits. In contrast, in the FRITIOF model multiple interactions are assumed to lead only to excitations of strings with greater mass. Many variations of the algorithm for multiple soft interaction are of course possible as emphasized before. The one implemented in HIJING is simply a minimal model which reproduces essential features of moderate energy pA and AA data.

The number of binary collisions at a given nuclear impact parameter is determined by Glauber geometry. We employ three-parameter Woods-Saxon nuclear densities determined by electron scattering data [105] to compute that geometry as done in ATTILA [15].

For each binary collision, we use the eikonal formalism as given in the previous section to determine the collision probability, elastic or inelastic, and the number of jets it produces. After a hard scattering, the energy of the scattered partons is subtracted from the nucleon and only the remaining energy is used to process the soft string excitation. The excited string system minus the scattered hard partons

suffers further collisions according to the geometric probabilities.

For each hard scattering, one then has to take into account the corrections due to initial and final state radiations. In an axial gauge and in the leading logarithmic approximation, the interference terms of the radiation drop out. The amplitude for successive radiations has then a simple ladder structure and the probability for multiple emissions becomes the product of each emission [97]. The virtualities of the radiating partons are ordered along the tree, decreasing until a final value μ_0^2 is reached below which pQCD is no longer valid. This provides the framework for a Monte Carlo simulation of parton showering and its space-time interpretation [106, 107].

At a given vertex of the branching tree, the probability for the off-shell parton a of virtuality $q^2 < q^2_{\max}$ to branch into partons b and c with fractions z and $1-z$ of the light-cone momentum is given by [106, 107]

$$d\mathcal{P}_{a\to bc}(q^2,z) = \frac{dq^2}{q^2} dz\, P_{a\to bc}(z) \frac{\alpha_s[z(1-z)q^2]}{2\pi} \frac{\mathcal{S}_a(q^2_{\max})}{\mathcal{S}_a(q^2)}, \tag{77}$$

where $P_{a\to bc}(z)$ is the Altarelli-Parisi splitting function [42] for the process $a \to bc$. By requiring the relative transverse momentum q_T of b and c to be real,

$$q_T^2 = z(1-z)\left(q^2 - \frac{q_b^2}{z} - \frac{q_c^2}{1-z}\right) \geq 0, \tag{78}$$

and a minimum virtuality $q_b^2,\ q_c^2 \geq \mu_0^2$, the kinematically allowed region of phase space is then,

$$\begin{aligned} 4\mu_0^2 < \quad & q^2 \quad < q^2_{\max}; \\ \epsilon(q) < \quad & z \quad < 1-\epsilon(q), \quad \epsilon(q) = \frac{1}{2}(1-\sqrt{1-4\mu_0^2/q^2}). \end{aligned} \tag{79}$$

Note that the '+function' and δ-function due to virtual corrections in the splitting functions in Eqs. (43)-(46) are not in effect in the allowed phase space. Their role has been replaced by the Sudakov form factor $\mathcal{S}_a(q^2)$ which is defined as [106, 107]

$$\mathcal{S}_a(q^2) = \exp\left\{-\int_{4\mu_0^2}^{q^2} \frac{dk^2}{k^2} \int_{\epsilon(k)}^{1-\epsilon(k)} dz \sum_{b,c} P_{a\to bc}(z) \frac{\alpha_s[z(1-z)k^2]}{2\pi}\right\}, \tag{80}$$

so that $\Pi_a(q^2_{\max}, q^2) = \mathcal{S}_a(q^2_{\max})/\mathcal{S}_a(q^2)$ is the probability for parton a not to have any branching between $q^2_{\max}$ and q^2. Therefore, the Sudakov form factor in the Monte Carlo simulation is essential to include virtual corrections and ensure unitarity. Since

the probability of parton emission between q^2 and $q^2 - dq^2$ is

$$\frac{dq^2}{q^2}\int_{\epsilon(k)}^{1-\epsilon(k)} dz \sum_{b,c} P_{a\to bc}(z)\frac{\alpha_s[z(1-z)q^2]}{2\pi}\ , \tag{81}$$

the probability of no parton emission, by unitarity, will be

$$1 - \frac{dq^2}{q^2}\int_{\epsilon(k)}^{1-\epsilon(k)} dz \sum_{b,c} P_{a\to bc}(z)\frac{\alpha_s[z(1-z)q^2]}{2\pi}\ , \tag{82}$$

between q^2 and $q^2 - dq^2$. The probability of no parton emission between $q^2_{\max}$ and $q^2 - dq^2$ then will be the product of the two probabilities,

$$\begin{aligned}\Pi_a(q^2_{\max}, q^2 - dq^2) &= \Pi_a(q^2_{\max}, q^2) - d\Pi_a(q^2_{\max}, q^2) \\ &= \Pi_a(q^2_{\max}, q^2)\left\{1 - \frac{dq^2}{q^2}\int_{\epsilon(k)}^{1-\epsilon(k)} dz \sum_{b,c} P_{a\to bc}(z)\frac{\alpha_s[z(1-z)q^2]}{2\pi}\right\}\end{aligned} \tag{83}$$

This is just another form of Eq. (77) integrated over z. One can see that the Sudakov form factor [106] is the solution of the above equation in which unitarity plays an important role.

In principle, one can perform the simulation of initial state radiation processes in a similar way. The partons inside a nucleon can initiate a space-like branching increasing their virtuality from some initial value Q_0^2. A hard scattering can be considered as a probe which can only resolve partons with virtuality up to the scale of the hard scattering. Otherwise without the scattering, the off-shell partons are only virtual fluctuations inside the hadron and they will reassemble back to the initial partons. In PYTHIA, which uses backward evolution, a hard scattering is selected first with the known QCD-evolved structure function at that scale, and then the initial branching processes are reconstructed down to the initial scale Q_0^2. The evolution equations are essentially the same as in final state radiation except that one has to convolute with the parton structure functions [17]. HIJING explicitly uses subroutines from PYTHIA to simulate each hard parton scattering and the associated initial and final state radiations. The initial virtuality for the initial state evolution is set to be Q_0 =2 GeV/c, and the minimum virtuality for the final state radiation is μ_0 = 0.5 GeV/c. The maximum virtuality for the associated radiations in a hard scattering with transverse momentum transfer p_T is chosen to be $q_{\max} = 2p_T$. Angular ordering can also be enforced in PYTHIA to take into account the soft gluon interference [107] in the final state radiation.

After all binary collisions are processed, the scattered gluons from each nucleon

are arranged according to their rapidities and connected to the valence quarks and diquarks of that nucleon in the collision. The rare hard scatterings of q-$\bar{q}$ pairs with opposite flavors are treated as a special case and processed as independent strings.

As studied in Refs. [108, 109, 110], large p_T partons must propagate transversely through the whole excited matter. They will suffer both elastic and radiative energy loss. The energy loss dE/dz is very sensitive to the Debye screening mass in the medium. Thus, the study of the energy loss of the produced hard jets or jet quenching can provide us with a unique probe of the dense matter. To test the sensitivity of final observables to jet quenching, we used a simple gluon splitting scheme (an effective induced radiation) in HIJING, given dE/dz and the mean free path of the interaction λ_f. The interactions are mostly soft between both soft and hard partons in the medium. These interactions and induced radiation, in some way, mimic pre-equilibrium cascading and semi-thermalization of the produced partons.

Induced radiative energy loss is modeled in HIJING by determining first the points of final state interaction of hard partons in the transverse direction and performing a collinear gluon splitting at every point. We assume that interactions only occur with the locally comoving matter in the transverse direction. Interactions with the nuclear fragments are negligible, because the two nuclear discs pass each other on a very short time scale $2R_A/\gamma \ll 1$ fm. The interaction points are determined by a probability with a constant mean free path λ_f,

$$dP = \frac{d\ell}{\lambda_f} e^{-\ell/\lambda_f}, \tag{84}$$

where ℓ is the distance the jet has traveled in the transverse direction after its last interaction.

Since the pre-hadronization state in HIJING is represented by connected groups (strings) of valence partons and gluons (kinks), interactions can be easily simulated by transferring a part of the parton energy, $\Delta E(\ell) = \ell dE/dz$, from one string configuration to another. Collinear gluon splitting results in a net jet quenching at the stage of hadronization, because the original hard parton energy is shared among several independent strings. This simple mechanism of course conserves energy and momentum and is numerically simple. A more dynamical parton cascade approach involving the space-time development of parton showering and collisions between the produced partons has been made in PCM [20].

To make sure that the model incorporates the right physics down to low energies we have compared the numerical results in pA and AA collisions with data at SPS energies. Shown in Fig. 12 are the calculated rapidity distributions of negative charged particles in pp (dot-dashed histogram), pAr (dashed histogram) and pXe

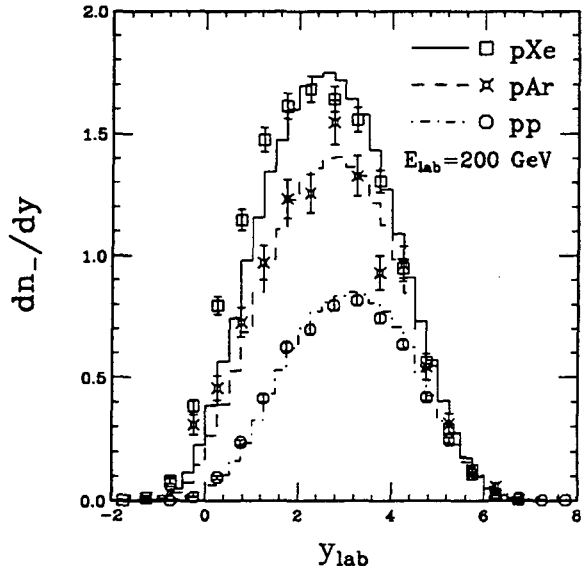

Figure 12: Rapidity distributions for negative particles in pp (circle, dot-dashed histogram), pAr (crossed-square, dashed histogram)and pXe (square, solid histogram) collisions at $E_{\rm lab} = 200$ GeV. The points are data from Ref. [111] and histograms are from HIJING calculation.

(solid histogram) collisions at $E_{\rm lab} = 200$ GeV. The data are from Ref. [111]. Because jet production is negligible at this energy, particle production occurs mainly through soft excitations of projectile and target nucleons. The HIJING low p_T algorithm reproduces an increase of particle production in the central region with the number of participating target nucleons. The peak of the rapidity distribution is shifted back towards the target region and its height is proportional to the target atomic number. In the target region, HIJING under-predicts particle production due to the neglect of final state cascading.

Shown in Figs. 13 and 14 are the calculated rapidity distributions of negative particles in central $O + Au$ collisions at $E_{\rm lab} = 60$ and 200 AGeV, and the transverse momentum distributions of negative particles in $p + p$ and central $O + Au$ collisions at $E_{\rm lab} = 200$ AGeV. The overall features of the data[112] are well accounted for except for the enhancement at low $p_T < 0.2$ GeV/c in $O + Au$. That enhancement is currently believed to originate also from final state interactions [113, 114]. The data for the $O + Au$ collisions are taken with a central trigger. In HIJING simulations, central events are selected which can give the corresponding averaged multiplicity.

The calculated results for central $Au + Au$ collisions at $\sqrt{s}$ =200 AGeV are shown in Fig. 15. The left panel shows the pseudorapidity distributions of charged particles. Note that without minijets (dotted), the $2A$ soft beam jets in HIJING

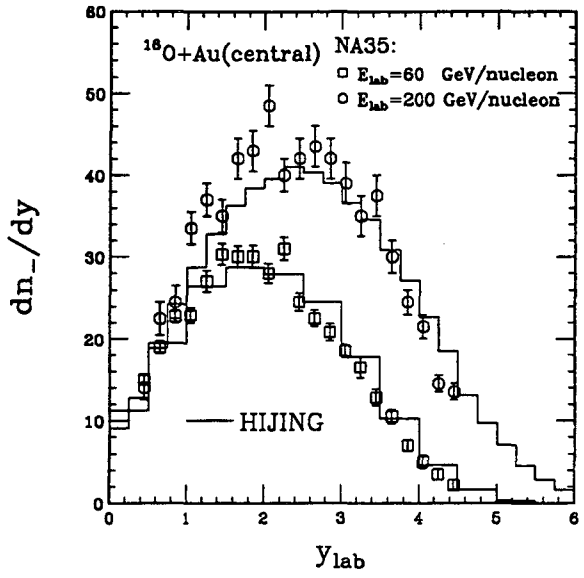

Figure 13: Rapidity distributions for negative particles in central $O + Au$ collisions at $E_{\rm lab} = 60$ and 200 AGeV. The data are from Ref. [112] and histograms are from HIJING calculation.

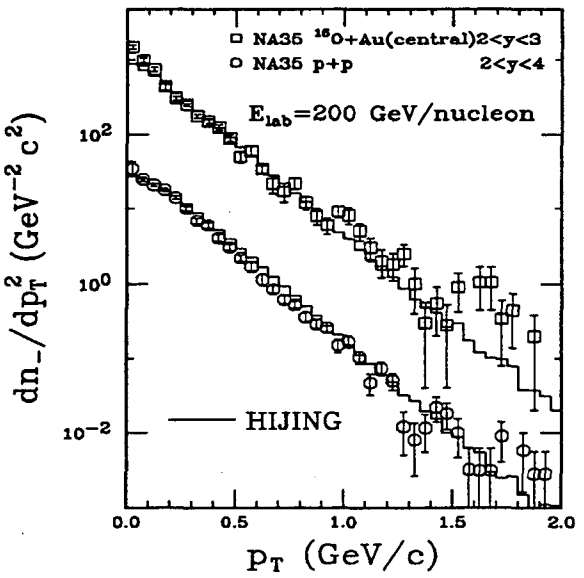

Figure 14: p_T distributions for negative particles in pp and central $O + Au$ collisions at $E_{\rm lab} = 200$ AGeV. The data are from Ref. [112] and histograms are from HIJING calculation.

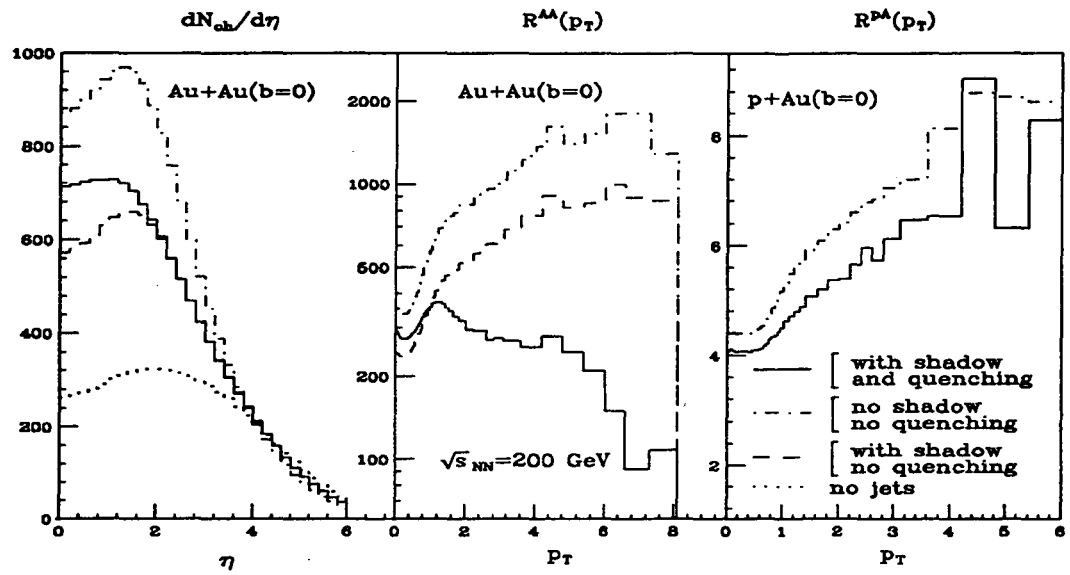

Figure 15: HIJING results of the dependence of the inclusive charged hadron spectra in central $Au + Au$ and $p + Au$ collisions on minijet production (dash-dotted), gluon shadowing (dashed), and jet quenching (solid) assuming that gluon shadowing is identical to that of quarks and dE/dz =2 GeV/fm with λ_f =1 fm. $R^{AB}(p_T)$ is the ratio of the inclusive p_T spectrum of charged hadrons in $A + B$ collisions to that of $p + p$.

lead to $dN_{AA}/d\eta \approx AdN_{pp}/d\eta$. Each beam jet contributes about 0.75 to the central rapidity density almost independent of energy [74]. Without gluon shadowing(dash-dotted), minijets are found to approximately triple the rapidity density due to beam jets. However, if gluon shadowing is of the same magnitude as that for quarks and antiquarks, then the minijet contribution to the rapidity density is reduced by approximately a half (dashed). The solid histogram shows that the effect of jet quenching on the rapidity density is small for $dE/dz = 2$ GeV/fm and λ_f =1 fm.

Plotted in the middle panel of Fig. 15, is the ratio,

$$R^{AB}(p_T) = \frac{d^2N_{AB}/dp_T^2/d\eta}{d^2N_{pp}/dp_T^2/d\eta}, \tag{85}$$

of the inclusive p_T spectrum of charged particles in central $Au + Au$ collisions to that of $p + p$. For $p_T > 2$ GeV/c, both shadowing and quenching are seen to reduce dramatically the inclusive hadron production. In the absence of shadowing and jet quenching (dash-dotted) the ratio approaches the number of binary pp collisions in the reaction. Shadowing alone (dashed) suppresses moderate p_T hadrons by a factor of about 2. Inclusion of jet quenching with $dE/dz = 2$ GeV/fm reduces that yield by

Ernest Orlando Lawrence Berkeley National Laboratory
One Cyclotron Road | Berkeley, California 94720

Prepared for the U.S. Department of Energy under Contract No. DE-AC03-76SF00098